From streamline jumping to strange eigenmodes: Bridging the Lagrangian and Eulerian pictures of the kinematics of mixing in granular flows

Ivan C. Christov,[1,a)] Julio M. Ottino,[2,3,4,b)] and Richard M. Lueptow[2,c)]
[1]*Department of Engineering Sciences and Applied Mathematics, Northwestern University, Evanston, Illinois 60208, USA*
[2]*Department of Mechanical Engineering, Northwestern University, Evanston, Illinois 60208, USA*
[3]*Department of Chemical and Biological Engineering, Northwestern University, Evanston, Illinois 60208, USA*
[4]*The Northwestern Institute on Complex Systems (NICO), Northwestern University, Evanston, Illinois 60208, USA*

(Received 16 May 2011; accepted 7 September 2011; published online 24 October 2011)

Through a combined computational–experimental study of flow in a slowly rotating quasi-two-dimensional container, we show several new aspects related to the kinematics of granular mixing. In the Lagrangian frame, for small numbers of revolutions, the mixing pattern is captured by a model termed "streamline jumping." This minimal model, arising at the limit of a vanishingly thin surface flowing layer, possesses no intrinsic stretching or streamline crossing in the usual sense, yet it can lead to complex particle trajectories. Meanwhile, for intermediate numbers of revolutions, we show the presence of naturally persistent granular mixing patterns, i.e., "strange" eigenmodes of the advection-diffusion operator governing the mixing process in Eulerian frame. Through a comparative analysis of the structure of eigenmodes and the corresponding Poincaré section and finite-time Lyapunov exponent field of the flow, the relationship between the Eulerian and Lagrangian descriptions of mixing is highlighted. Finally, we show how the mapping method for scalar transport can be modified to include diffusion. This allows us to examine (for the first time in a granular flow) the change in shape, lifespan, and eventual decay of eigenmodes due to diffusive effects at larger numbers of revolutions. © *2011 American Institute of Physics*. [doi:10.1063/1.3653280]

I. INTRODUCTION

Granular flows open a window into a complex, disordered system far from equilibrium exhibiting both chaotic dynamics and self-organization,[1] amongst a variety of other behaviors.[2] Recently, new aspects of the short-time kinematics of granular flow have been uncovered in three-dimensional containers slowly rotated about two axes.[3] While, in a granular flow in a rotating tumbler, all stretching (in the sense of continuum mechanics) occurs in a thin surface fluidized shear layer (the *flowing layer*), mixing and complicated particle trajectories can be observed even when the flowing layer becomes vanishingly thin.[3–6] This can be considered an example of complex dynamics without the "usual symptoms" of chaos and related[3,5,6] to the mathematical concept of a *piecewise isometry* (PWI).[7–10] Because such complex dynamics do not arise from the usual "stretching and folding" mechanism of chaotic mixing, the new mechanism has been termed[3] "cutting and shuffling," a tip to the similarity between PWIs and the "mixing" of a deck of cards.[11] However, many questions remain as to the extent of PWI dynamics in the vanishing-flowing-layer limit and the implications for mixing and transport in granular (and related) flows.

In the first part of this paper, we focus on the Lagrangian description of mixing, i.e., on how to understand the motion of material points in this continuum. In doing so, we extend the result of Juarez *et al.*[3]—that the dynamics under the model with a vanishingly thin flowing layer represents the "skeleton" of mixing in experiments—to quasi-two-dimensional (quasi-2D) non-circular containers with variable fill fractions. In particular, we present experimental evidence for the underlying mixing mechanism of *streamline jumping*,[5,6] which has been studied only theoretically so far, and we relate this description of the mixing process to previous models of avalanching and continuous granular flow in a rotating container.

Such dynamics is readily observable in granular mixing in slowly rotated containers for *small* numbers of revolutions;[3] on longer time scales, however, the effects of Lagrangian coherent (morphological) structures created by advection cannot be ignored.[12] When diffusive effects are weak, these structures can give rise to *naturally persistent mixing patterns*, sometimes called "strange" eigenmodes, which can be understood in terms of the Eulerian description of mixing. Such Eulerian coherent structures, first observed in numerical simulation of advective-diffusive transport in idealized flows[13] and subsequently in fluid mixing experiments,[14–17] have generated significant interest in recent years. Mathematically, a strange eigenmode is just a dominant eigenmode of the advection-diffusion operator governing the mixing of a passive scalar in a flow.[18] Such eigenmodes can have an intricate spatial structure that oscillates and persists for long times. At first, this was unexpected; hence, the reason for having been dubbed "strange."

[a)]Electronic mail: christov@u.northwestern.edu. URL: http://alum.mit.edu/www/christov
[b)]Electronic mail: jm-ottino@northwestern.edu. URL: http://mixing.chem-biol-eng.northwestern.edu
[c)]Author to whom correspondence should be addressed. Electronic mail: r-lueptow@northwestern.edu.

Recently, Singh *et al.*[19] revisited the issue of strange eigenmodes using a simple numerical approach to distributive mixing, originally studied by Spencer and Wiley,[20] and found that the eigenmodes of the advection operator (diffusion is neglected in this approach) can be obtained from the eigenvectors of a so-called mapping or distribution matrix. In the second part of this paper, we use the simplified mapping method[21] and the spectral structure (i.e., the eigenvalue-eigenvector pairs) of its distribution matrix to present the first study of both strange eigenmodes and distributive scalar transport by the mapping method in the context of tumbling granular flows in rotating containers. In addition, through an analysis of the flow based on Lagrangian diagnostics such as the Poincaré section and the finite-time Lyapunov exponent (FTLE) field, we relate the spatial organization of the (Eulerian) eigenmodes to coherent flow structures such as the Kolmogorov–Arnold–Moser (KAM) islands that surround elliptic periodic points, and the invariant manifolds of hyperbolic periodic points.

Unlike molecular diffusion in fluid mixing, however, diffusive effects in granular mixing manifest quickly[22] due to the significant contribution of dissipative inter-particle collisions in the flowing layer.[23] Thus, while studies of strange eigenmodes in fluids[14–17] are mainly concerned with how a mixing pattern saturates to a particular combination of eigenmodes, granular mixing adds a new dimension to the phenomenon: namely, the destruction of naturally persistent patterns by diffusion. In the third part of this paper, we present a novel extension of the mapping method to include diffusion. We use the latter to show that a finite superposition of dominant *advective-diffusive* eigenmodes manifest themselves in experiments with *both* monodisperse and bidisperse granular materials. It is observed that diffusion not only changes their structure (compared to purely advective eigenmodes) but also reduces the timescale on which they can be observed in a tumbled monodisperse granular system.

II. KINEMATICS OF THE FLOW

A. Continuum model of granular flow in a tumbler

Under the original model of Khakhar *et al.*,[22] the (Eulerian) velocity field $\boldsymbol{u} = u_x\hat{\boldsymbol{\imath}} + u_y\hat{\boldsymbol{\jmath}}$, in the moving frame of a tumbler with arbitrary convex shape (see Fig. 1), takes the form

$$u_x(x,y,t) = \begin{cases} 2\bar{v}_x(t)[1 + y/\delta(x,t)], & y > -\delta(x,t), \\ \omega_z[y + h(t)] - \dot{g}(t), & \text{otherwise}, \end{cases} \tag{1a}$$

$$u_y(x,y,t) = \begin{cases} -\omega_z x[y/\delta(x,t)]^2, & y > -\delta(x,t), \\ -\omega_z[x + g(t)] - \dot{h}(t), & \text{otherwise}, \end{cases} \tag{1b}$$

where a superimposed dot indicates a time derivative, and $\omega_z(>0)$ is the *clockwise* rotation rate. Here,

$$\delta(x,t) = \delta_0(t)\left\{1 - [x/L(t)]^2\right\}, \quad \bar{v}_x(t) = \frac{\omega_z L(t)^2}{2\delta_0(t)} \tag{2}$$

are, respectively, the instantaneous flowing layer depth and the instantaneous depth-averaged flowing layer streamwise velocity, which is assumed to be independent of x in this model. The continuum is incompressible and thus $\boldsymbol{\nabla}\cdot u = 0$, as can be verified from Eqs. (1) and (2). In numerical simulations, Eq. (1) is transformed to a rigid coordinate system (aligned with the walls of the container in its initial orientation) by the change of variables $x \to \tilde{x} - g(t)$, $y \to \tilde{y} - h(t)$, where $g(t)$ and $h(t)$ are the horizontal and vertical (signed) distances, respectively, between the center of rotation C and the midpoint of the free surface O (see Fig. 1).

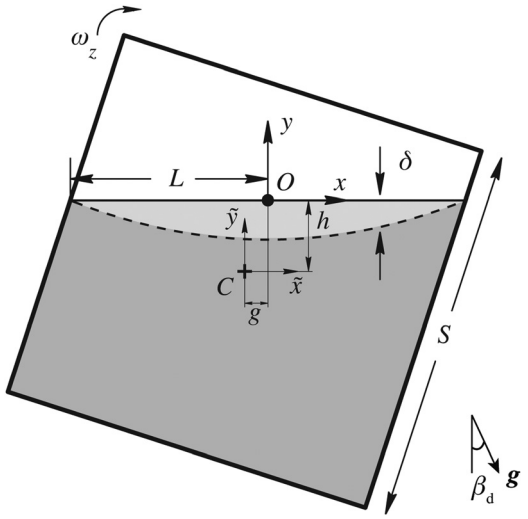

FIG. 1. Diagram of a 70% full square quasi-2D tumbler, which has been rotated backwards by the dynamic angle of repose β_d (so that the free surface of the flow is horizontal), showing the coordinate systems and notation. The out-of-plane thickness of the tumbler is assumed much smaller than its width and height, so it is not shown. The boundary between the flowing layer (light gray) and the bulk (dark gray) is represented by a dashed curve. Adapted, with permission, from I. C. Christov, J. M. Ottino, and R. M. Lueptow, "Streamline jumping: A mixing mechanism," Phys. Rev. E **81**, 046307 (2010). © 2010 American Physical Society.

Here, for a given convex tumbler shape, the maximal depth of the flowing layer $\delta_0(t)$ and the half-length of the free surface $L(t)$ are known functions of time (i.e., orientation) alone and are such that $\epsilon := \delta_0(t)/L(t)$ can be assumed to be a constant independent of time.[22] This is termed the *geometric similarity* of the flowing layer because, physically, it means that the flowing layer adjusts instantaneously to changes in the container's orientation. Thus, the free parameters are the flowing layer's aspect ratio ϵ and the container's fill fraction ϕ. (Once the tumbler's shape and ϕ are specified, the time-dependent quantities h, g and L can be determined.) Finally, the flow period is defined as $T = (2\pi/\omega_z)/\mathfrak{n}$, where $\mathfrak{n}$ is the number of sides in the case of a polygonal tumbler.[24,25]

B. The vanishing-flowing-layer limit and the avalanching-to-continuous-flow transition

Four distinct regimes of granular flow in a tumbling mixer can be identified.[26,27] At very small rotation rates, the flow is in the "avalanching" regime (Fig. 2(a)), for which a wedge model was proposed by Metcalfe *et al.*[28,29] Meanwhile, at larger (though still small) rotation rates, the flow enters the "continuous/rolling/cascading" regime (Fig. 2(b)), which was modeled by Khakhar *et al.*[22,30] As discussed in

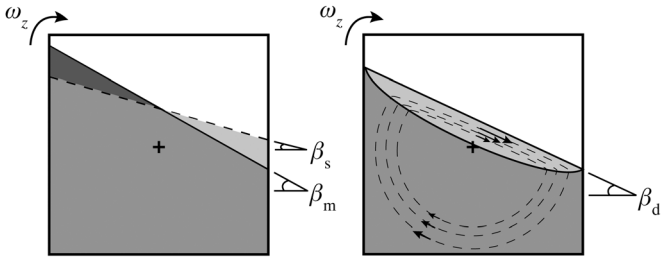

FIG. 2. Diagrams of two granular flow regimes in a square tumbler. In the avalanching regime (a), the flow consists of intermittent avalanches. Whenever the free surface reaches the marginal angle of repose β_m, the dark gray wedge of material upstream flows down the slope becoming the light gray wedge. Now, the free surface is at the static angle of repose $\beta_s < \beta_m$. As the tumbler continues to rotate, the process repeats. In the continuous-flow regime (b), the flow consists of a thin fluidized surface layer. The free surface remains almost flat and maintains an angle, the dynamic angle of repose β_d, with respect to the horizontal. The angles β_m, β_s, and β_d are constants that depend on both the properties of the granular material (e.g., particle size and surface roughness) and the tumbler (e.g., axial depth and rotation rate) (Ref. 27).

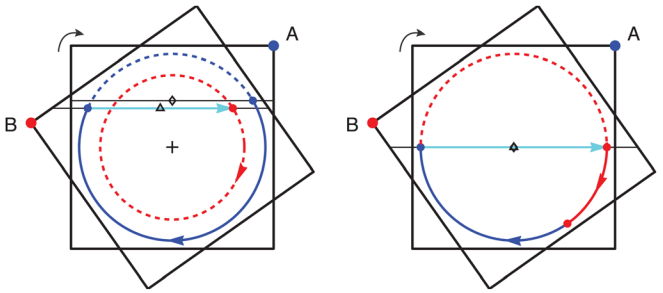

FIG. 3. (Color online) In a 73% full square tumbler (a), a particle initially on the solid blue streamline can transfer to the dashed red streamline, as the tumbler rotates from orientation A to B, by jumping across the infinitely thin flowing layer (light blue arrow). This is because the location of the free surface's midpoint is different between orientations A (small diamond) and B (small triangle). For a 50% full square tumbler (b), however, the midpoint of the free surface remains fixed and no streamline jumping is possible. Particle trajectories coincide with the solid-body-rotation streamline they start on. Adapted, with permission, from I. C. Christov, J. M. Ottino, and R. M. Lueptow, "Chaotic mixing via streamline jumping in quasi-two-dimensional tumbled granular flows," Chaos **20**, 023102 (2010). © 2010 American Institute of Physics.

Sec. II A, this is the regime we are most interested in. Even though the transition from intermittent avalanches to continuous flow is quite complicated,[31,32] these simple models describe each case quite faithfully insofar as mixing is concerned.

At the interface between these two models lies the limiting case of a vanishingly thin flowing layer. The latter, when framed mathematically as the limit of $\epsilon \equiv \delta_0(t)/L(t) \to 0$, exhibits streamline jumping, and the kinematics can be described by a nonlinear map that is the composition of isometries.[5,6] In this limit, it can be shown that the flowing layer becomes vanishingly thin (specifically, an interface at the free surface), while the time-of-flight through the flowing layer goes to zero because the magnitude of the mean surface velocity diverges as $1/\epsilon$. [5,6] Then, streamline jumping becomes possible: particle trajectories undergoing solid body rotation can switch their radius from the center of rotation C by jumping across the midpoint of the free surface instantaneously, i.e., $(x,y) \to (-x,y)$.

To illustrate this, let us move to the fixed frame with origin at C. Now, consider a material point $(\tilde{x}_m, \tilde{y}_m)^\top$ in the right-half of the infinitely thin flowing layer (coincident with the free surface in Fig. 1), which is located at some $g(t_m) < \tilde{x}_m < L(t_m) + g(t_m)$ and $\tilde{y}_m = h(t_m)$ at time $t = t_m$. Then, its trajectory returns to the right-half of the flowing layer at some later time t_{m+1} given implicitly by $h(t_{m+1}) = r_0 \sin(\theta_0 - \omega_z(t_{m+1} - t_m))$, where $r_0 = (\tilde{x}_m^2 + \tilde{y}_m^2)^{1/2}$ and $\theta_0 = \tan^{-1}(\tilde{y}_m/\tilde{x}_m)$. Then, this material point's trajectory is the composition of three isometries—a rotation, a reflection and a translation—and takes the form[5,6] (see also Ref. 4):

$$\tilde{x}_{m+1} = -\cos(\omega_z \bar{t})\tilde{x}_m - \sin(\omega_z \bar{t})\tilde{y}_m + 2g(t_{m+1}), \tag{3a}$$

$$\tilde{y}_{m+1} = -\sin(\omega_z \bar{t})\tilde{x}_m + \cos(\omega_z \bar{t})\tilde{y}_m, \tag{3b}$$

where $\bar{t} := t_{m+1} - t_m$. The last term in Eq. (3a) represents translation. Notice that t_{m+1} (and, hence, $\bar{t}$) is implicitly a function of $\tilde{x}_m$ and $\tilde{y}_m$, making the map described by Eqs. (3) a nonlinear generalization of the piecewise isometries (PWIs) from the pure mathematics literature.[7–10] Figure 3 illustrates, at two different tumbler fill levels, typical trajectories defined by Eq. (3), including streamline jumping in Fig. 3(a).

One way to understand *physically* the type of process that the limiting system describes is to consider what happens as the rotation rate ω_z of the tumbler is increased past the critical value at which avalanching gives way to continuous flow. The transition has been found to exhibit hysteresis[31] and intermittency,[32] which makes the definition of a single critical angular velocity impossible. But suppose, for the sake of argument, that some estimate (ω_z^{crit}) can be made. Then, as $\omega_z \to (\omega_z^{crit})^-$ the wedges of the discrete avalanching model[28,29] become thinner and avalanche more often. Eventually, they become infinitely thin (zero area but finite length) and the flow becomes continuous (as opposed to intermittent).[4,33,34] Then, as ω_z passes through ω_z^{crit}, a flowing layer of finite depth develops and the flow becomes continuous in time.

Put this way, the continuous avalanching of infinitely thin wedges described above is precisely streamline jumping.[5,6] This suggests that the mathematical framework resulting from taking the limit of a vanishing-flowing-layer is not an idealization but a model of granular flow in a specific, albeit very small, range of rotation rates. Nevertheless, it is a particularly useful regime to understand, because (as has been suggested before[3,5,6] and is reinforced in Sec. III) it provides the "skeleton" of mixing when the flowing layer is thin, as is often the case in real granular flows.[27]

Finally, just as the wedge-based avalanche model predicts no mixing for certain 50% full tumblers[28,29] (e.g., ones with circular or even-sided polygonal cross-sections), streamline jumping (in continuous flow with an vanishingly thin flowing layer) is also impossible in these 50% full tumblers because the resulting map in Eq. (3) is trivial.[5,6] Thus, the wedge and streamline jumping models are consistent with one another at the intersection of their respective applicability.

III. THE VANISHING-FLOWING-LAYER LIMIT: EXPERIMENT AND SIMULATION

Here, for the purposes of illustrating the quasi-2D vanishing-flowing-layer dynamics, we use a square tumbler. However, those features of mixing under this flow that we elucidate are generic to convex non-circular tumblers (e.g., polygonal ones).[24,25] Note that, in this section, we study the mixing process in the Lagrangian frame by seeding an initial assortment of tracers of different colors and then tracking their re-arrangement due to the flow.

Figures 4, 5, and 6 show, for three different fill fractions of the example square quasi-2D tumbler, comparisons between experiments (see Appendix A) and simulations of the mixing pattern (see Appendix B) with a flowing layer of comparable thickness ($\epsilon = 0.1$), a very thin flowing layer ($\epsilon = 0.01$) and a vanishingly thin flowing layer ($\epsilon = 0$). This illustrates to what extent the $\epsilon = 0$ behavior (streamline jumping) can be observed in a monodisperse quasi-2D granular mixing experiment. In the experiments, the flowing layer has a maximum thickness $\delta_0(0)$ of 6 ± 1 particle diameters, consistent with a previous investigation.[35] The tumbler's side length and particles' diameters are, respectively, $S = 25$ cm $(= 2L(0))$ and $d = 2.03 \pm 0.04$ mm (combined uncertainty of black and clear particles, see Appendix A), hence $\epsilon \equiv \delta_0(0)/L(0) = 0.10 \pm 0.02$. Noting that the model is not sensitive to small changes in this parameter,[6] we take $\epsilon = 0.1$ in the numerical simulations of the case with a flowing layer of realistic thickness.

From Fig. 4, it is immediately clear that for a fill fraction $\phi = 0.5$, the $\epsilon = 0$ dynamics is trivial and periodic. Indeed, at this fill fraction, streamline jumping (the mechanism of mixing for $\epsilon = 0$) is impossible and all particles remain on their initial streamlines.[5,6] By comparing the simulations with a thin (but non-zero thickness) flowing layer to the experiment, it is evident that a finite-thickness flowing layer leads to the interface between the black and clear particles becoming slanted. This does not, however, lead to mixing of the black and clear particles even after 10 flow periods (quarter revolutions of the container). (The impact of granular diffusion becomes noticeable when comparing the simulation with $\epsilon = 0.1$ to the experiments, particularly on the left side of the tumbler, though the interface between black and clear

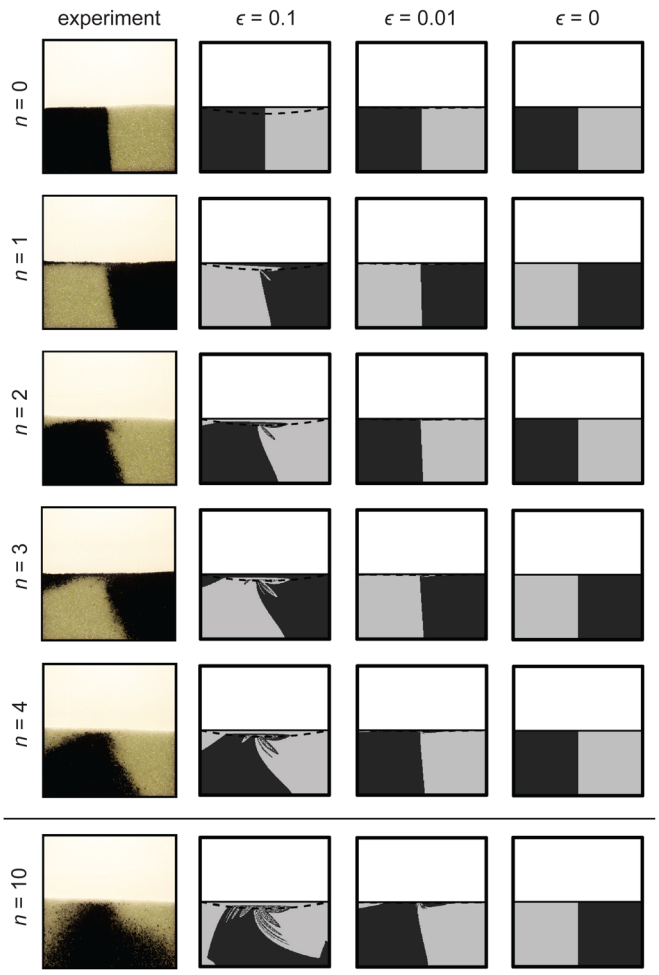

FIG. 4. (Color online) A 50% full quasi-2D square tumbler, rotated backwards by the dynamic angle of repose, after n quarter-revolutions. At this fill fraction, the dynamics corresponding to $\epsilon = 0$ (the "skeleton" of mixing) is trivial. Simulations with a finite-thickness flowing layer (the dashed curve evident for $\epsilon = 0.1$) and the experiment likewise show that the region of black particles deforms somewhat, yet no significant mixing occurs.

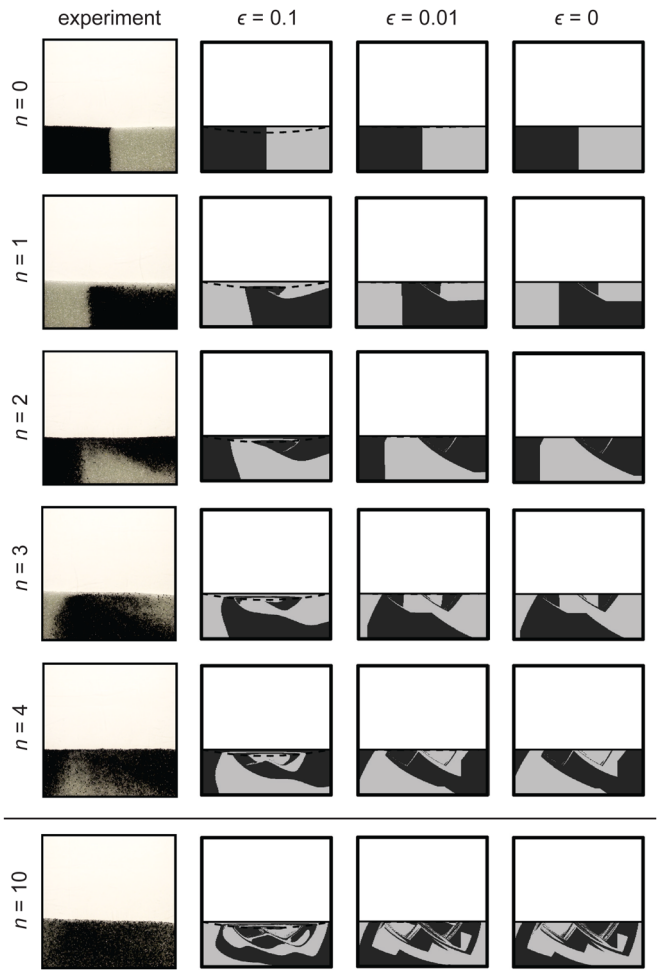

FIG. 5. (Color online) A 35% full quasi-2D square tumbler rotated backwards by the dynamic angle of repose. The initially segregated pattern is "cut and shuffled" into a collection of intricate structures. Simulations with a finite-thickness flowing layer show the effects of stretching due to shear are negligible, and that streamline jumping (the $\epsilon = 0$ dynamics) is the primary stirring mechanism in the flow for low numbers of flow periods.

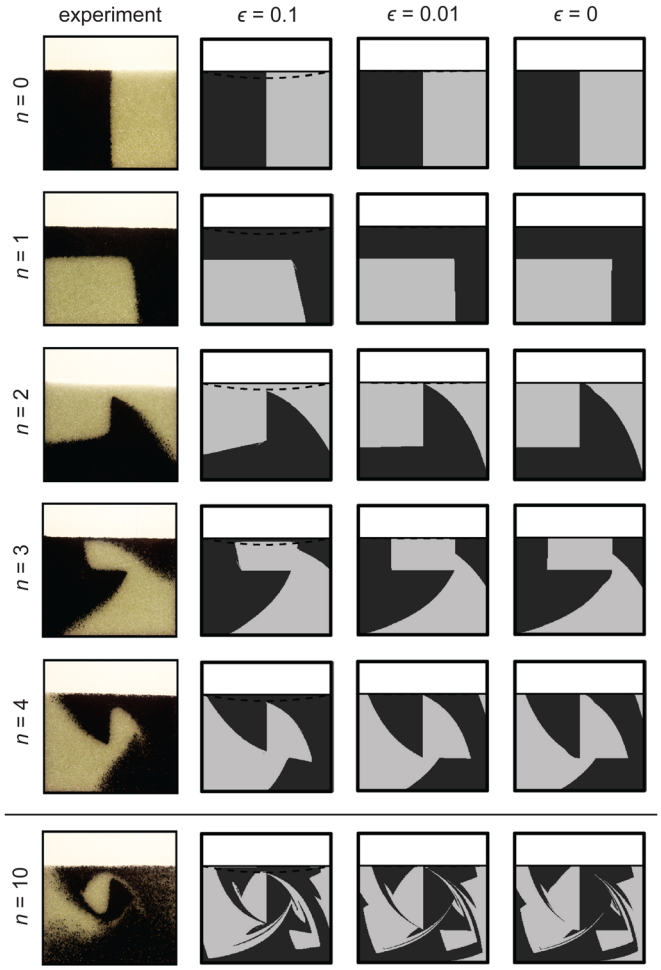

FIG. 6. (Color online) A 75% full quasi-2D square tumbler rotated backwards by the dynamic angle of repose. Due to the presence of an unmixed core at this fill fraction, the effect of streamline jumping on the initially (unmixed) pattern is easy to observe. Simulations with a finite-thickness flowing layer show that the effects of stretching in the flowing layer are negligible, with the $\epsilon = 0$ dynamics being the primary feature of the flow for many periods. Once again, the experimental results show the role of diffusion becomes apparent by $n \approx 10$.

particle remains distinct and fairly sharp.) Therefore, we can conclude that the lack of streamline jumping is readily observable at this stage of the process. The $\epsilon = 0$ behavior in this case is analogous to the $\pi/2 - \pi/2$ PWI map in the half-full three-dimensional blinking spherical tumbler.[3]

In Fig. 5, for $\phi = 0.35$, complex behavior can be observed. Although it is clear that the $\epsilon = 0$ dynamics is the "skeleton" of the flow, by $n = 4$ the simulation with a realistic flowing layer $(\epsilon = 0.1)$ and the experiment look somewhat different. As we show in Sec. V B, the diffusive effects of inter-particle collisions in the flowing layer are quite significant in this case, since at such low fill fractions the particles go through the flowing layer more often than at higher fill fractions. At $n = 10$, the granular material in the experiment appears well-mixed, which is not surprising given the degree of mixing in the simulations together with granular diffusion. However, it is still remarkable that to a large extent the vanishing-flowing-layer dynamics can be observed in the finite-thickness flowing layer simulations and the experiments for the first few periods.

Finally, the case of $\phi = 0.75$ is illustrated in Fig. 6. For such fill fractions greater than 0.5 (specifically, those such that $h - \delta_0 > 0$), it is expected that overall mixing is reduced because of the existence of an unmixed core, which consists of particles that never pass through the flowing layer.[28] At this fill fraction, it is quite easy to distinguish the three fundamental mixing processes in the granular flow:[36] streamline jumping (a mechanism related to PWIs[5,6] and cutting and shuffling[3]), stretching and folding (due to shear in the flowing layer[1,22]), and diffusion (due to inter-particle collisions in the flowing layer[23]). Streamline jumping leads to the initially rectangular regions of black and clear (more precisely, light gray in the simulation plots) particles becoming intricate, curved regions with sharp edges. Stretching and folding is initially very weak in this case, even for $\epsilon = 0.1$, but leads to certain parts of the black/clear particle interface becoming slanted (evident at $n = 1,2,3$ and similar to the case of $\phi = 0.5$ in Fig. 4). Note that thin filamentary structures are observed even for $\epsilon = 0$ because streamline jumping leads to spreading of material points and complex patterns even in the absence of stretching (in the sense of shear strain) within the flowing layer.[6] Diffusion can also be observed in the experimental images as parts of the interface become "fuzzier" with each iteration, though the diffusive effects are relatively weak for small n. Even at $n = 10$, some of the $\epsilon = 0$ dynamics can be distinguished in the experimental image. Thus, the minimal model represented by streamline jumping provides the skeleton of the mixing pattern in a (monodisperse) granular flow.

IV. ADVECTIVE-DIFFUSIVE SCALAR TRANSPORT

A. Mathematical setting

So far we have only considered the mixing problem from the Lagrangian viewpoint: tracking the advection of passive tracer particles of different colors to determine what occurs in a tumbled granular system. A complementary approach is the Eulerian viewpoint, whereby one studies the spatiotemporal evolution of the concentration c, on some two-dimensional domain $\Omega \subset \mathbb{R}^2$, under the advection-diffusion equation

$$\frac{\partial c}{\partial t} + \boldsymbol{u} \cdot \nabla c = \frac{1}{\mathrm{Pe}} \nabla^2 c, \quad \boldsymbol{x} \in \Omega, \quad t > 0, \tag{4a}$$

$$\hat{\boldsymbol{n}} \cdot \nabla c = 0, \quad \boldsymbol{x} \in \partial\Omega, \quad t > 0, \tag{4b}$$

where Pe is the Péclet number, $\hat{\boldsymbol{n}}$ is the outward unit normal to the boundary $\partial\Omega$, and the velocity field is assumed solenoidal and time-periodic: $\nabla \cdot \boldsymbol{u} = 0$ and $\boldsymbol{u} = \boldsymbol{u}(\boldsymbol{x}, t) = \boldsymbol{u}(\boldsymbol{x}, t + T) \forall t$. In what follows, c can be either the concentration of black or clear particles, depending on the particular situation under consideration.[37] The Péclet number is defined as the ratio of the advective to the diffusive time scales, i.e., $\mathrm{Pe} \equiv \ell U/D$, where ℓ is the characteristic length of the domain, U is a characteristic velocity of the flow, and D is the diffusivity of the tracer. In addition, there is the initial condition $c(\boldsymbol{x},0) = c_0(\boldsymbol{x})$, which we suppose is such that $\int_\Omega c_0(\boldsymbol{x})\, d\boldsymbol{x} = M$, where M is a given constant (the "mass" of the tracer). Moreover, due to the no-flux (Neumann) boundary condition in Eq. (4b):[38]

$$\int_\Omega c(\boldsymbol{x},t)\,\mathrm{d}\boldsymbol{x} \equiv M \quad \forall t \geq 0, \tag{5}$$

i.e., the "mass" of the tracer is conserved.

For any bounded velocity field with general time dependence, Liu and Haller[18] have shown that the concentration profile quickly converges to a (finite-dimensional) inertial manifold spanned by, say, N dominant eigenmodes of the advection-diffusion operator $\mathcal{L} \equiv -\boldsymbol{u}\cdot\boldsymbol{\nabla} + \mathrm{Pe}^{-1}\boldsymbol{\nabla}^2$. These dominant eigenmodes are the building blocks of the naturally persistent patterns[39] that were termed strange eigenmodes.[13] The spectral theory of linear operators[40,41] and Floquet theory for partial differential equations[18] have provided significant insight into the structure of naturally persistent mixing patterns. Numerical simulations have shown even more contexts in which they exist, e.g., in electro-hydrodynamic flow induced in droplets,[42] in the mixing flows of certain non-Newtonian fluids,[39,43] in periodically reoriented potential flows,[44] and in heat transfer during mixing.[45]

Thus, we may express[46] the concentration field as the linear superposition

$$c(\boldsymbol{x},t) \approx \frac{M}{|\Omega|} + \sum_{k=1}^{N-1} \alpha_k \varphi_k(\boldsymbol{x};t)\mathrm{e}^{\lambda_k t}, \tag{6}$$

where $|\Omega|$ is the area of the domain, α_k is the kth expansion coefficient determined from the initial condition, and $\varphi_k(\boldsymbol{x};t)$ is the kth eigenfunction with corresponding eigenvalue λ_k defined as

$$\mathcal{L}[\varphi_k(\boldsymbol{x};t)] = \lambda_k \varphi_k(\boldsymbol{x};t), \quad k = 0,\ldots,\infty. \tag{7}$$

Following Singh *et al.*,[19] the kth *eigenmode* is defined as $\hat{\varphi}_k(\boldsymbol{x};t) = \varphi_k(\boldsymbol{x};t)\mathrm{e}^{\lambda_k t}$. Note that, due to the time dependence of $\boldsymbol{u}$, the eigenfunctions depend on time as a parameter with $\varphi_k(\boldsymbol{x};t) = \varphi_k(\boldsymbol{x};t+T)\forall t$. Clearly, those eigenmodes that have a λ_k with a small real part decay the slowest with t; hence, they are termed "most dominant" or "most persistent." Note that $Re\{\lambda_k\} \leq 0$ for all k since the Eq. (4a) is dissipative,[40] i.e., there are no eigenmodes that grow without bound in time. Also, the summation in Eq. (6) starts at $k=1$ because $\{\varphi_0,\lambda_0\} = \{M/|\Omega|,0\}$ is always an eigenfunction-eigenvalue pair due to the no-flux (Neumann) boundary condition.

Since we are dealing with a time-periodic flow, it is helpful to shift the discussion to *discrete-time* quantities. To this end, we introduce the *Floquet operator* $\mathcal{F}$ [19,40] defined through

$$\mathcal{F}[c(\boldsymbol{x},t)] = c(\boldsymbol{x},t+T) \quad \forall t. \tag{8}$$

Then, the Floquet eigenfunctions $\psi_k(\boldsymbol{x})$ are defined as

$$\mathcal{F}[\psi_k(\boldsymbol{x})] = \mu_k \psi_k(\boldsymbol{x}), \quad k = 0,\ldots,\infty. \tag{9}$$

The analog of Eq. (6) in terms of these quantities is

$$c(\boldsymbol{x},nT) \approx \frac{M}{|\Omega|} + \sum_{k=1}^{N-1} \beta_k \psi_k(\boldsymbol{x})\mu_k^n, \tag{10}$$

where c is a discrete-time quantity now, i.e., it can be evaluated only at multiples n of the flow period T. As before, the kth eigenmode is defined as $\hat{\psi}_k(\boldsymbol{x};n) = \psi_k(\boldsymbol{x})\mu_k^n$, and the expansion coefficients $\{\beta_k\}_{k=1}^{N-1}$ are determined from the initial condition $c_0(\boldsymbol{x})$. Writing the eigenmodes this way, it is clear that each has a repeating spatial structure as given by ψ_k, and this structure can oscillate in time and decay in accordance with $|\mu_k|^n$. Those eigenmodes with $|\mu_k|$ closest to unity are the most dominant ones, and $|\mu_k| \leq 1$ for all k, since the concentration profile cannot grow without bound with n.

Again, it is easy to see that $\{\psi_0,\mu_0\} = \{M/|\Omega|,1\}$ is always an eigenfunction-eigenvalue pair due to the conservation of mass. Hence, if Eq. (5) is to be satisfied, then from Eq. (10) we must have that $\int_\Omega \psi_k(\boldsymbol{x})\,\mathrm{d}\boldsymbol{x} = 0$ for any $k>0$. Thus, the constant eigenmode $\hat{\psi}_0(\boldsymbol{x};n) \equiv \mu_0^n\psi_0(\boldsymbol{x}) = \psi_0(\boldsymbol{x})$ is referred to as the "homogeneous" one, while the remaining eigenmodes ($\hat{\psi}_k$ for $k>0$) are referred to as "inhomogeneous."[19] For finite Pe, μ_0 is the only eigenvalue of $\mathcal{F}$ that can equal one in magnitude because the equation is dissipative. Finally, though some of the eigenvalues can be complex, they must come in conjugate pairs since $\mathcal{F}$ is a real-valued operator. Hence, the concentration profile in Eq. (10) is always a real quantity.

B. Numerical implementation via the mapping method

The mapping method for scalar transport was initially developed to circumvent the issue of high-precision tracking of material lines (a difficult numerical problem[47]) when studying the transport properties of a stirring flow. For the time being, we restrict to the case of vanishing diffusion (i.e., $\mathrm{Pe} \to \infty$), meaning we consider purely distributive mixing as done by Singh *et al.*[19] An accurate mapping matrix can be constructed by discretizing the domain into a regular grid (see Fig. 7) and then tracking how much of the material in each cell is transported to every other cell, say over a single period of the flow.[48–50] Recently, an efficient way of computing the distribution matrix from Lagrangian trajectories has been developed,[21] leading to a faster and more versatile implementation suitable for the optimization of micromixers.[51]

In a tumbled granular system, the domain Ω changes in time since the container is rotating. Therefore, a faithful approximation of the partial differential Eq. (4a) appears to be difficult, though methods for (stationary) curved geometries have been developed.[42] Indeed the standard mapping method (based on interfacial tracking) is known to fail for

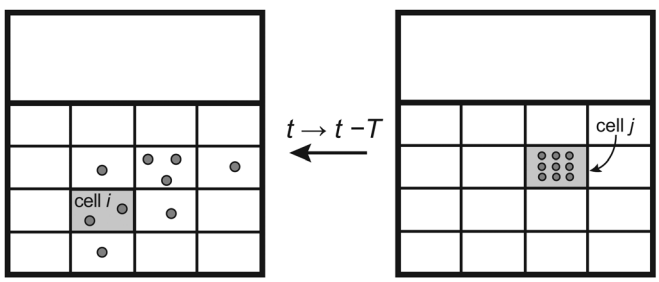

(a) tracers one period earlier (b) current location of tracers

FIG. 7. Illustration of how the filled portion of the example quasi-2D square tumbler is discretized. Here, $N_x = N_y = 4$ and 3^2 tracers are seeded in all cells before the tracking begins. From Eq. (11), we see that $\boldsymbol{\Phi}_{ij} = 2/9$ in this example. Note that the cells are rectangles when $N_x = N_y$ (and $\phi \neq 0$ or 1), and this is the case for all numerical simulations presented in what follows.

mixers with complicated geometries.[21,39,43] Additionally, Galerkin methods developed[40] for approximating the Floquet operator in Eq. (8) that are based on Fourier series do not readily extend to our problem. The simplified mapping method in Fig. 7, on the other hand, requires only the knowledge of where Lagrangian particle trajectories start and end over one period of the flow. This kind of particle tracking can be easily implemented for granular flows in a tumbler.[6,24]

To this end, the domain Ω (assuming that Ω at $t=0$ coincides with Ω at $t=T$) is divided into a grid of cells, each one with a certain number of passive tracers uniformly distributed throughout its area. The passive tracers are advected from $t=T$ back to $t=0$ (see the discussion in Appendix B), whence the components of the distribution matrix $\mathbf{\Phi}$ are

$$\Phi_{ij} = \frac{\text{number of tracers in cell } j \text{ that came from cell } i}{\text{total number of tracers seeded in cell } j}. \tag{11}$$

Denoting by c the vector of mean values of c over the cells of the discretized domain, the concentration grid function c^n after n periods is computed recursively from the previous one(s):

$$\boldsymbol{c}^n = \mathbf{\Phi}\boldsymbol{c}^{n-1} = \cdots = \mathbf{\Phi}^n\boldsymbol{c}^0. \tag{12}$$

For computational efficiency, powers of the matrix are not computed (since $\mathbf{\Phi}$ is sparse but its powers are, generally, not). Instead, the matrix is applied repeatedly. Here, $\mathbf{\Phi}$ is an $(N_xN_y)\times(N_xN_y)$ matrix, where N_x and N_y are, respectively, the number of cells in x and y directions, and c^n is an $(N_xN_y)\times 1$ vector. Henceforth, for simplicity, we let $N=N_xN_y$ be the total number of cells of the grid, which is also the number of eigenmodes that can be resolved on it. Then, the distribution matrix $\mathbf{\Phi}$ constitutes a discrete approximation (for $\mathrm{Pe}=\infty$) of the Floquet operator $\mathcal{F}$ defined in Eq. (8) and $c_j^n \approx c(\boldsymbol{x}_j, nT)$, where $\boldsymbol{x}_j$ are the centers of the cells and c_j^n is the jth component of $\boldsymbol{c}^n$.

C. A modification of the mapping method that includes diffusion

Applying the Marchuk–Yanenko operator splitting scheme (see, e.g., Sec. 30 in Ref. 52) to Eq. (4a), it can be formally discretized in time (taking a time step equal to the period) as

$$\frac{\boldsymbol{c}^* - \boldsymbol{c}^n}{T} = \mathcal{L}_1^h\boldsymbol{c}^*, \quad \frac{\boldsymbol{c}^{n+1} - \boldsymbol{c}^*}{T} = \mathcal{L}_2^h\boldsymbol{c}^{n+1}, \tag{13}$$

where $\boldsymbol{c}^*$ is an intermediate quantity, and we have used the fact that $\mathcal{L}$ can be decomposed into the sum of $\mathcal{L}_1 = -\boldsymbol{u}\cdot\nabla$ and $\mathcal{L}_2 = \mathrm{Pe}^{-1}\nabla^2$; an h superscript denotes that the operator has been discretized in space. Here, T is the flow period made dimensionless by the advection timescale as dictated by the non-dimensionalization of Eq. (4a); we return to the issue of timescales in Sec. V B. The solution of the first equation is precisely the goal of the mapping method described above, i.e., $\boldsymbol{c}^* = \mathbf{\Phi}\boldsymbol{c}^n$. Then, the second equation in (13) can be rewritten as

$$\left(\mathbf{I} - T\mathcal{L}_2^h\right)\boldsymbol{c}^{n+1} = \mathbf{\Phi}\boldsymbol{c}^n, \tag{14}$$

and its solution is readily obtained:

$$\boldsymbol{c}^{n+1} = \left(\mathbf{I} - T\mathrm{Pe}^{-1}\mathbf{\Delta}^h\right)^{-1}(\mathbf{\Phi}\boldsymbol{c}^n), \tag{15}$$

where we take $\mathbf{\Delta}^h$ to be the standard 5-point finite-difference approximation to the Laplacian modified for zero Neumann boundary conditions (see, e.g., Sec. 1.2 in Ref. 53), and $\mathbf{I}$ is the identity matrix. Defining $\widetilde{\mathbf{\Phi}} = (\mathbf{I} - T\mathrm{Pe}^{-1}\mathbf{\Delta}^h)^{-1}\mathbf{\Phi}$, the analysis by Singh *et al.*[19] of the spectral structure of the advection-diffusion (*not* just the pure advection) problem and the strange eigenmodes can be immediately carried out. Clearly, in the limit of $\mathrm{Pe}\to\infty$ the usual mapping matrix and method are recovered (i.e., $\lim_{\mathrm{Pe}\to\infty}\widetilde{\mathbf{\Phi}} = \mathbf{\Phi}$).

Formally, the unconditional stability of the implicit treatment of the diffusion and advection[54] operators allows us to take the time step equal to the period T, though if we were to solve the PDE in Eq. (4a) in such a manner we would commit a large splitting error. Here, we only use the *conceptual framework* of operator splitting to motivate our approach; we make no claims this is a highly accurate method for solution of PDEs. Moreover, even though no numerical analysis of the purely advective mapping method has been performed in the literature, the method has been quite successful. We argue this is also likely to be the case for our modification of the mapping method to include diffusion. In fact, the initial work[13,55] on the subject successfully employed a similar approach of applying one period of an advection operator, followed by one period of a diffusion operator.

It is important to note that, for granular flows in tumblers, operator splitting with a time step of one period T makes sense physically because only material in the flowing layer is subject to diffusion at any given time. The material in the bulk of solid body rotation is in static equilibrium and does not experience diffusion. However, during one period of the flow, most material goes through the flowing layer, thereby experiencing the effects of diffusion. Hence, taking a time step equal to T ensures the advection-diffusion model in Eq. (4a) is consistent with the physics of this granular flow.

As we demonstrate below through comparisons with experiments, $\widetilde{\mathbf{\Phi}}$ is a numerically accessible analogue of Eq. (8) at finite Pe. For the purposes of exploring, the qualitative nature of eigenmodes, this numerical approach is sufficiently accurate when enough cells are used in constructing the grid, and enough tracers are seeded in each cell; convergence is checked by doubling the grid size and ensuring the structure of the eigenmodes remains unchanged.

V. EIGENMODE ANALYSIS OF GRANULAR FLOW IN A SQUARE TUMBLER

A. Existence and structure of advective (Pe = ∞) granular strange eigenmodes

First, it is important to stress that the eigenmodes are generic features of advection-diffusion in the presence of the underlying velocity field as given in Eq. (1) (the "normal modes" of the process, so to say), and they are independent of the initial condition used in a mixing simulation/experiment.

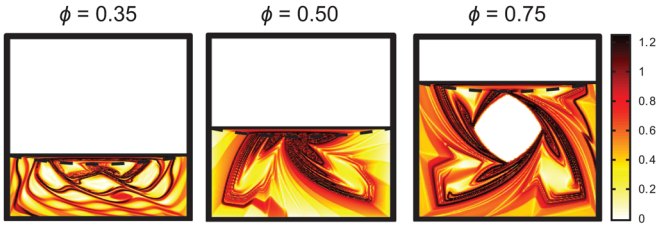

(a) FTLE field with respect to $t = -14T$

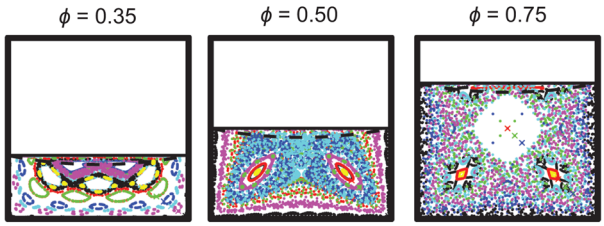

(b) Poincaré section over 500 periods

FIG. 8. (Color online) Transport diagnostics of granular flow in a square tumbler with a flowing layer (dashed curves) of realistic thickness ($\epsilon = 0.1$) at the three example fill fractions we study.

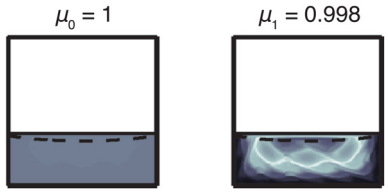

(a) the most dominant real eigenmodes

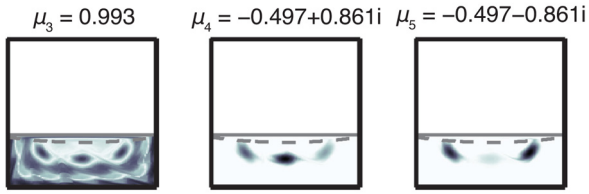

(b) eigenmodes corresponding to a period-3 island chain

FIG. 9. (Color online) Representative purely advective ($\mathrm{Pe} = \infty$) eigenmodes $\hat{\psi}_k(\boldsymbol{x}; 0)$ of the concentration field of the granular flow in a quasi-2D tumbler with $\phi = 0.35$ and $\epsilon = 0.1$ (flowing layer is the dashed curve) shown in Fig. 5, as approximated by the eigenvectors of the mapping matrix $\boldsymbol{\Phi}$.

As we show below, they manifest themselves in both simulations and experiments.

To better understand the structure of eigenmodes of granular flow in a rotating tumbler, it is first helpful to examine the underlying kinematic transport features of the flow under the paradigm of *chaotic advection*.[56] To this end, we consider the dynamical system generated by the velocity field in Eq. (1)[5,6] and present two kinds of computational results.

First is the finite-time Lyapunov exponent (FTLE) fields, or maximum local length stretch,[57] shown in Fig. 8(a) for the three fill fractions in the model square tumbler. Ridges (a type of locally–maximizing curve) of the FTLE field have been proposed as both indicators[58] for and possibly a definition[59] of *Lagrangian coherent structures* (LCS),[60] which are material surfaces of maximum (or minimum) stretching in the flow. Under certain mathematical restrictions on the flow, such LCS can represent finite-time approximations of the unstable manifolds of hyperbolic points.[58] However, to properly identify an LCS in a flow of arbitrary time dependence one must show that further conditions (beyond being a ridge of the FTLE field) are satisfied.[61] For the time-periodic flow we study, the highest ridges (darkest curves in the plots in Fig. 8(a)) are the invariant unstable manifolds of hyperbolic periodic points. This can be verified by comparing to the manifold traces in Fig. 12 of Meier *et al.*[25] It is important to stress that not all ridges are part of the unstable manifolds;[6] some may be the result of strong shear rather than hyperbolicity.[62]

Second, we consider long-time Poincaré sections of the dynamical system (i.e., stroboscopic maps in which the location of tracer is plotted after every period of the flow), as shown Fig. 8(b). These reveal the global transport dynamics, specifically KAM islands surrounding elliptic periodic points (i.e., regions of regular dynamics, punctuating an otherwise chaotic domain, that persist thanks to the KAM theorem[57]). Both the FTLE fields and the Poincaré sections are Lagrangian diagnostics of the flow, and (as shown below) they play an important role in interpreting (in a sense, a roadmap to) the Eulerian coherent structures represented by eigenmodes.

Figures 9 and 10 show the eigenstructure of two tumbled granular systems. Each eigenmode's normalization is arbitrary, so a color scale is not shown. It suffices to note that the absolute value is plotted, meaning what is presented is the "intensity" of the eigenmode. For complex-conjugate pairs of eigenmodes, the absolute values of the real and imaginary

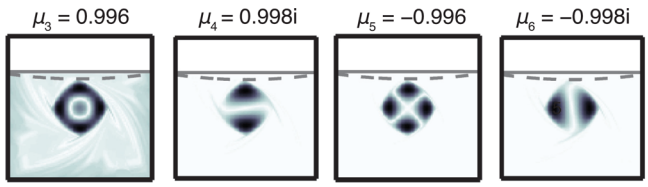

(a) period-4 eigenmodes within the unmixed core

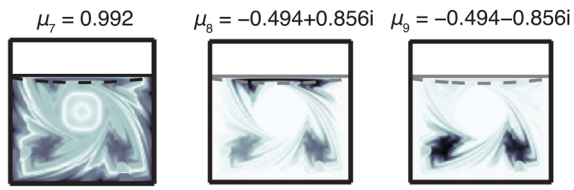

(b) eigenmodes corresponding to a period-3 island chain

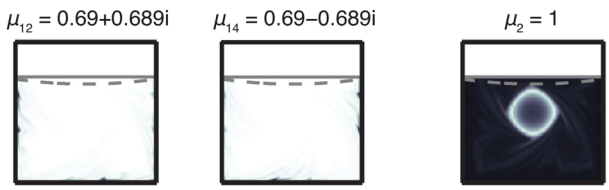

(c) conjugate pair from a period-8 group in the chaotic region

(d) asymptotic state of unmixed core

FIG. 10. (Color online) Representative purely advective ($\mathrm{Pe} = \infty$) eigenmodes $\hat{\psi}_k(\boldsymbol{x}; 0)$ of the concentration field of granular flow in a quasi-2D tumbler with $\phi = 0.75$ and $\epsilon = 0.1$ shown in Fig. 6, as approximated by the eigenvectors of the mapping matrix $\boldsymbol{\Phi}$.

parts are plotted. Consequently, white regions correspond to $\hat{\psi}_k \approx 0$, while in the dark regions $\hat{\psi}_k$ is non-zero. Following Singh *et al.*,[19] let us also introduce the following terminology: regions where $\hat{\psi}_k \not\approx 0$ that contribute to the evolution are termed *active*, while those regions where $\hat{\psi}_k \approx 0$ and those with $\hat{\psi}_k \approx const.$ that do not contribute to the evolution are termed *inactive*.

It is useful to make the distinction between eigenmodes that comprise chaotic regions and those that comprise chains of KAM islands. By Conjecture 3 of Singh *et al.*,[19] chaotic and KAM regions must be "spatially disconnected" from each other, making the corresponding eigenmodes easy to pick out visually. Furthermore, a period-p structure (e.g., period-p KAM island chain) will be composed of the eigenvectors corresponding to eigenvalue clusters of the form $|\mu_{k+m}|e^{i\pi m/p}$ for $m=0,\ldots,\ p-1$, where $e^{i\pi m/p}$ are the pth roots of unity and $|\mu_{k+m}| = |\mu_k|$ for $m=0,\ldots,p-1$ in the absence of diffusion. These are the so-called *subharmonic* eigenmodes.[18]

In Fig. 9(a), the leading (ordered by the magnitude of $|\mu_k|$) two eigenmodes of the flow in a 35% full tumbler are shown. As suggested by the theoretical analysis, $\mu_0 = 1$, and the corresponding eigenmode is homogenous. The next most-dominant eigenmode, $\hat{\psi}_1$, has a real eigenvalue and its active region delineates a number of KAM islands seen in the Poincaré section in the left panel of Fig. 8(b). This is the naturally persistent pattern we would expect to observe in an experiment. Indeed, in the mixing simulation shown in Fig. 5 with $\epsilon = 0.1$ and $n = 10$, this pattern is beginning to emerge. In the experiment, however, this pattern cannot be distinguished visually because diffusion has led to significant decay of this eigenmode's amplitude. We consider the effects of diffusion on eigenmodes in Sec. V B.

Furthermore, notice that the lighter regions of $\hat{\psi}_1$ (where this eigenmode would be termed "less active") clearly foreshadow Fig. 9(b). In the latter, a triplet of eigenmodes, which corresponds to the KAM island chain revealed by the Poincaré section in the left panel of Fig. 8(b) and observed in the mixing simulations in Fig. 5, is shown. The third roots of unity are $\left\{1, -\frac{1}{2}+\frac{\sqrt{3}}{2}i, -\frac{1}{2}-\frac{\sqrt{3}}{2}i\right\}$, and in Fig. 9(b), we observe the eigenvalues μ_3, μ_4, and μ_5 are precisely these roots, but with their overall magnitude damped by a factor of approximately 0.98 to 0.99. This is an artifact of "numerical diffusion."[63] Nevertheless, it is clear this is a persistent feature of the mixing pattern in the absence of diffusion. It is interesting to note that the complex pair ($\hat{\psi}_4$ and $\hat{\psi}_5$) of this triplet is clearly active only in the KAM island chain while the remaining eigenmode ($\hat{\psi}_3$), which has a corresponding real eigenvalue, is "leaky," i.e., its active region delineates other island chains beyond the period-3 one it belongs to, in contrast to Conjecture 5 ("The active zones of all eigenvectors…combined demarcate the invariant region occupied by the entire period p group…") of Singh *et al.*[19] This could be a manifestation of aliasing in the numerical method, as all such period- p eigenmodes have one real positive eigenvalue near 1, so the eigenmodes corresponding to these eigenvalues can, in a sense, be aliasing each other.

Figure 10 shows some representative eigenmodes for the 75% full tumbler. The group of eigenmodes with eigenvalues $\approx \{1,i,-1,-i\}$ (with magnitude slightly less than one due to numerical diffusion) in Fig. 10(a) represents the persistent unmixed core observed in experiments at this fill fraction (recall Fig. 6 for $n = 10$). It is easy to see that this must be a period-4 structure by noting the four locations of tracers in the core part of the Poincaré section shown in the right panel of Fig. 8(b).

A period-3 KAM island chain can also be easily distinguished in the Poincaré section shown in the right panel of Fig. 8(b) by observing the red (see online version for color) tracer's trajectories on the lower main diagonals of the tumbler and in the center of the flowing layer. The corresponding triplet of eigenmodes is shown in Fig. 10(b). Again, we observe that the eigenmode with real eigenvalue in this group is "leaky" as was the case for the similar one in the 35% full tumbler.

Then, in Fig. 10(c), a pair of eigenmodes from a period-8 cluster in the chaotic region of the flow are depicted. (We know this is the chaotic region of the flow by consulting the corresponding Poincaré section in Fig. 8(b).) The eighth roots of unity are $\left\{1, \frac{1}{\sqrt{2}}+\frac{1}{\sqrt{2}}i, i, -\frac{1}{\sqrt{2}}+\frac{1}{\sqrt{2}}i, -1, -\frac{1}{\sqrt{2}}-\frac{1}{\sqrt{2}}i, -i, \frac{1}{\sqrt{2}}-\frac{1}{\sqrt{2}}i,\right\}$, and we can check that the angles of μ_{12} and μ_{14} match those of $-\frac{1}{\sqrt{2}}+\frac{1}{\sqrt{2}}i$ and $-\frac{1}{\sqrt{2}}-\frac{1}{\sqrt{2}}i$ (accounting for numerical diffusion). However, the active region of this pair of eigenmodes is very small, barely visible along the left wall and the bottom for $\hat{\psi}_{12}$ and symmetric with respect to the vertical centerline for $\hat{\psi}_{14}$. Diffusion has a significant effect on them, as we show in Sec. V B. Finally, Fig. 10(d) shows that there exists an additional non-decaying eigenmode (i.e., one with eigenvalue equal to 1). This is because, in the absence of diffusion, the unmixed core at this fill fraction persists forever. Therefore, for $t \to \infty$, the asymptotic advection pattern cannot be simply the homogeneous state, but some combination of it and the eigenmode in Fig. 10(d).

Finally, notice that the eigenmodes in the right panels of Figs. 10(b)–10(d) fit together, and the curves along which they fit are precisely the darkest ones in the FTLE plot in the right panel of Fig. 8(a), i.e., the finite-time traces of unstable manifolds. Similarly, the different regions in which the eigenmode in the right panel of Fig. 9(a) is active are clearly delineated by the corresponding highest FTLE ridges (with the eigenmode's least intensity being along them) from the left panel of Fig. 8(a). These are approximations of invariant curves across which there is no transport. Therefore, it makes sense that active regions of eigenmodes align with curves of largest local stretching, rather than cross them; on each side of these curves, the dynamics is different and the character of different dynamics is represented by different eigenmodes as we have argued above. This was also observed by Popovych *et al.*[64] for a stochastic time-periodic sine flow.

B. Effects of diffusion (finite Pe) on the structure of granular strange eigenmodes

Using the modification of the mapping method introduced in Sec. IV C, we can study the effects of tracer diffusivity on the existence and structure of eigenmodes from Sec. V A. As an introductory example, consider the real

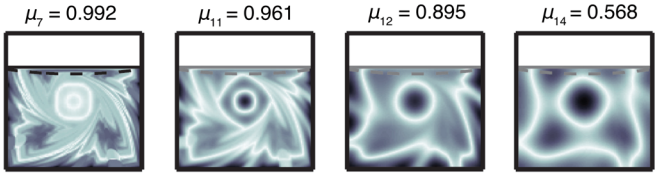

FIG. 11. (Color online) A progression (decreasing Péclet number from left to right) illustrating the effect of diffusion on one eigenmode from the period-3 cluster shown in the left panel of Fig. 10(b) (with $\phi = 0.75$ and $\epsilon = 0.1$), as approximated by the appropriate eigenvector of the modified mapping matrix $\widetilde{\mathbf{\Phi}}$.

eigenmode (in the left panel of Fig. 10(b)) from the triplet corresponding to a period-3 KAM island chain. Figure 11 shows the effect of decreasing Péclet number (i.e., increasing significance of diffusion) on this eigenmode. Diffusion destroys the fine-scale features of the eigenmode as Pe decreases from ∞ to 1000. The unmixed core and an outline of the extent of the period-3 islands, which this eigenmode corresponds to in the advection-only limit, are a persistent feature for all Pe shown. In addition, the eigenvalue corresponding to this eigenmode decreases with Pe to almost half its value at Pe = 1000 compared to Pe = ∞. We elaborate on these observations in the remainder of the paper.

Figure 11 clearly shows that the effects of diffusion on the structure of an eigenmode and the magnitude of its eigenvalue can be quite significant. Therefore, it is important to determine the proper Péclet number corresponding to typical granular flow laboratory experiments (such as those discussed in Sec. III). To this end, it is convenient to re-write the Péclet number explicitly as a ratio of timescales: $\mathrm{Pe}_{\mathrm{coll}} = (\ell_d^2/D)/(\ell_a/U) = \ell_d^2 U/(\ell_a D)$, where ℓ_a and ℓ_d are the advective and diffusive length scales, respectively, and D is the collisional diffusivity. To reconcile this re-definition of Pe with the one from Sec. IV A, where only a single length scale (the advective one) can be used, we note that $\mathrm{Pe}_{\mathrm{coll}} = (\ell_d/\ell_a)^2(\ell_a U/D) = (\ell_d/\ell_a)^2\mathrm{Pe}$. Since diffusive effects in a granular flow manifest themselves primarily as fluctuations in the depth (y-position) of particles due to their collisions as they pass through the flowing layer, it is natural to take the length scales to be[22,27] $\ell_a = L(0)$ and $\ell_d = \delta_0(0) \Rightarrow (\ell_d/\ell_a)^2 = \epsilon^2$. The characteristic velocity is then $U = \bar{v}_x(0)$, i.e., the maximum depth-averaged streamwise velocity defined in Eq. (2). Consequently, the expression for the flow period in Sec. IV C is $T = \frac{1}{4}(2\pi/\omega_z)/(\ell_a/U) = \pi/(4\epsilon)$. Defining the collisional diffusivity D is more difficult, however it can be done by matching the free parameter in Savage's model[65] of granular self-diffusion to experimental data.[22] This gives $D \approx 0.025 d^2\dot{\gamma}$, where d is the particle diameter and $\dot{\gamma}$ is the shear rate, for a quasi-2D monodisperse granular flow of glass beads with solid volume fraction of $\approx 55\%$, as in our experiments. Finally, the streamwise shear rate $\dot{\gamma}$ can be taken to be its maximum value at the free surface, i.e., $\dot{\gamma}(x = 0, t = 0) = \omega_z L(0)^2/\delta_0(0)^2$ as computed from Eq. (1a). Thus, we arrive at

$$\mathrm{Pe}_{\mathrm{coll}} \approx \frac{\delta_0(0)^2\left\{\omega_z L(0)^2/[2\delta_0(0)]\right\}}{L(0)0.025d^2\left\{\omega_z L(0)^2/\delta_0(0)^2\right\}} = 20\frac{\delta_0(0)^3}{L(0)d^2}. \quad (16)$$

This gives $\mathrm{Pe}_{\mathrm{coll}} = 70 \pm 35$ for the granular flows considered herein. Noting the approximate nature of Eq. (16) and that the eigenmode analysis is insensitive to the specific value of Pe, we use the order-of-magnitude estimate $\mathrm{Pe}_{\mathrm{coll}} \approx 100 \Rightarrow \mathrm{Pe} = \epsilon^{-2}\mathrm{Pe}_{\mathrm{coll}} \approx 10,000$ for the simulations in this subsection. Although this is a fairly large Péclet number, it suggests diffusion still plays a role in our granular mixing experiments, unlike many other engineering applications where Pe is even larger. For this reason, as was evident in Sec. III, it is difficult to obtain sharp experimental images after a large number of revolutions; granular diffusion blurs the boundaries between the two colors of particles being mixed.

With regard to the eigenmodes of a tumbled granular system, Fig. 12 is the equivalent of Fig. 9 but with Pe = 10,000 instead of ∞. First, in accordance with the theoretical considerations from Sec. IV A, we confirm that the homogeneous eigenmode $\hat{\psi}_0$ with eigenvalue $\mu_0 = 1$ persists in the presence of diffusion. However, the next most dominant eigenmode from Fig. 9(a) has been displaced by the complex-conjugate pair of eigenmodes shown in Fig. 12(b). We can see that precisely this pair of eigenmodes has been excited in the mixing experiment shown in Fig. 5 by noting where the clear particles go from $n = 3$ (showing $\hat{\psi}_2$) to $n = 4$ (showing $\hat{\psi}_3$). Their location corresponds approximately to the active region (dark) of the pair of eigenmodes from Fig. 12(b). Finally, in Fig. 12(c), the effects of diffusion on the period-3 KAM island chain from Fig. 9(b) can be seen. The KAM islands have become "leakier" as diffusion allows a flux through the previously invariant[66] unstable manifolds (recall Fig. 8(a)) that separate the chaotic from regular regions of the flow. Moreover, the magnitude of the eigenvalue cluster corresponding to the period-3 KAM island chain has been damped by diffusion, shortening the "lifespan" of these eigenmodes.

Similarly, for the 75% full tumbler, Fig. 13 is the equivalent of Fig. 10 but with Pe = 10,000. Once again we observe

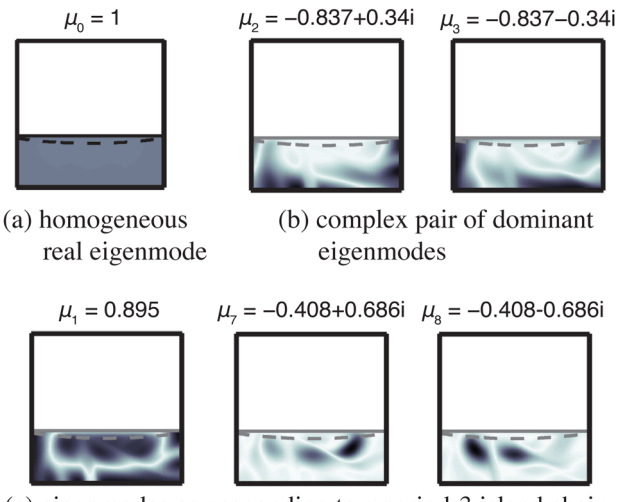

FIG. 12. (Color online) Advective-diffusive eigenmodes $\hat{\psi}_k(\boldsymbol{x}; 0)$ of the 35% full tumbler with $\epsilon = 0.1$, whose purely advective (Pe = ∞) eigenmodes are depicted in Fig. 9, approximated by the eigenvectors of the modified mapping matrix $\widetilde{\mathbf{\Phi}}$ with Pe = 10,000.

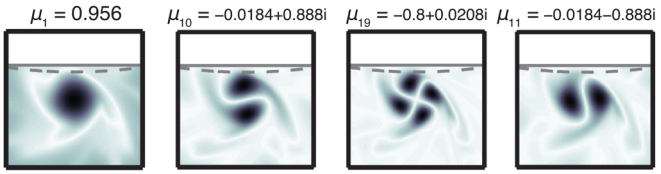

(a) period-4 eigenmodes within the unmixed core

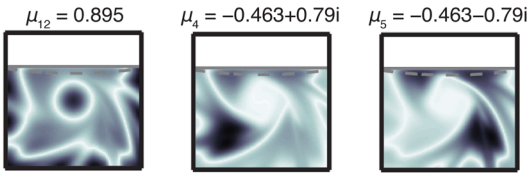

(b) eigenmodes corresponding to a period-3 island chain

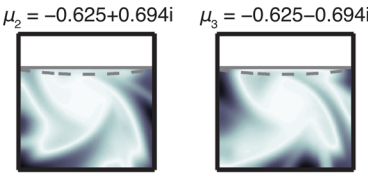

(c) conjugate pair from a period-8 group in the chaotic region

FIG. 13. (Color online) Advective-diffusive eigenmodes $\hat{\psi}_k(\boldsymbol{x};0)$ of the 75% full tumbler with $\epsilon = 0.1$, whose purely advective ($\mathrm{Pe} = \infty$) eigenmodes are depicted in Fig. 10, approximated by the eigenvectors of the modified mapping matrix $\widetilde{\boldsymbol{\Phi}}$ with $\mathrm{Pe} = 10{,}000$.

a much "leakier" chaotic region of the period-3 eigenmodes in Fig. 13(b) as compared to Fig. 10(b). What is more striking, however, is the extent of the active zones of the two eigenmodes from a period-8 chain depicted in Fig. 13(c). For $\mathrm{Pe} = \infty$ in Fig. 10(c), the active zone is barely distinguishable, while at $\mathrm{Pe} = 10{,}000$ it extends through a significant portion of the domain. Another observation is that $\hat{\psi}_{19}$ shown in the third panel of Fig. 13(a) is now one of a pair of complex-conjugate eigenmodes (we have shown only one of them), compared with $\hat{\psi}_5$ in the third panel of Fig. 10(a). As suggested by Singh *et al.*,[19] this is a numerical artifact, which disappears as $N \to \infty$, and the pair of computed eigenmodes corresponds to a single physical eigenmode. Finally, note that the eigenmode in Fig. 10(d), which represents the asymptotic state of an unmixed core, is no longer dominant. This is because, under Eq. (4a) with finite Pe, the asymptotic state cannot contain an unmixed core. The amplitudes of the eigenmodes corresponding to the core must eventually decay completely due to diffusion, leading to a homogeneous concentration distribution $\boldsymbol{c}(\boldsymbol{x},nT) \to M/|\Omega|\ \forall \boldsymbol{x} \in \Omega$ as $n \to \infty$.

C. Dominant exponents and their asymptotic scalings

The *characteristic decay time* of the kth eigenmode is defined as[19]

$$\tau_k = -\frac{T}{\ln|\mu_k|}. \tag{17}$$

Note that we assume $k > 0$ here because we always have $\mu_0 = 1$ for the homogeneous eigenmode, which is not "strange." Clearly, $\tau_k \to \infty$ as $|\mu_k| \to 1$ and $\tau_k \to 0$ as $|\mu_k| \to 0$. Thus, for good mixing, it is desirable that the spectrum of the Floquet operator $\mathcal{F}$ (or of its discrete approximation $\widetilde{\boldsymbol{\Phi}}$) has as few eigenvalues close to the unit circle as possible, so that the "lifespan" of the dominant eigenmodes is as short as possible.

Cerbelli *et al.*[40,41] define an analogous quantity: the *(most) dominant exponent* Λ, which we can write in terms of the characteristic decay time from Eq. (17) as

$$\Lambda = \frac{1}{\max_k \tau_k}. \tag{18}$$

This is a convenient quantity to use in studying the dependence on (finite) Péclet number of the eigenvalues of the advection-diffusion operator, as shown by Giona *et al.*[67] for the idealized time-periodic sine flow. However, the eigenmode with largest τ_k may not necessarily oscillate in time (as did the original strange eigenmodes[13]) if $\mathrm{Im}\{\mu_k\} = 0$. Therefore, it is useful to introduce an analogous quantity to the dominant exponent, denoted by Λ^*, for which the maximum in Eq. (18) is taken over all k for which $\mathrm{Im}\{\mu_k\} \neq 0$. Since complex eigenvalues originate from advection (in the case of pure diffusion, the operator $\mathcal{L}$ is self-adjoint and the Floquet operator $\mathcal{F}$ inherits this property[40]), quantifying the decay time of the most dominant oscillatory eigenmode using Λ^* gives a measure of the influence of advection on the mixing process. We expect that as $\mathrm{Pe} \to \infty$, we always have $\Lambda \to 0$, since in this limit, it is possible to have $\tau_k \to \infty$ for some $k \neq 0$ (i.e., there exist non-decaying inhomogeneous eigenmodes). Similarly, $\Lambda^* \to 0$ as $\mathrm{Pe} \to \infty$ is only possible when there is a pair of permanent eigenmodes with complex conjugate eigenvalues $\mu_{k+1} = \overline{\mu_k}$ such as those corresponding to a KAM island chain.

Although Eq. (16) shows that the Péclet number and the maximal flowing layer thickness $\delta_0(0)$ (equivalently, the flowing layer's aspect ratio $\epsilon \equiv \delta_0(0)/L(0)$) are not independent quantities in an experiment, it is nevertheless instructive to suppose ϵ is fixed but we can vary Pe. That is, given a granular flow with some specified velocity field (with ϕ and ϵ known and fixed) as in Eq. (1), we would like to know what is the effect of Pe on the characteristic decay time of eigenmodes.

To this end, Fig. 14 shows the scaling of Λ and Λ^* with Pe for granular flow in a square tumbler at the three chosen fill fractions ϕ as the flowing layer's aspect ratio ϵ is varied. The plots suggest that the scaling is relatively independent of ϕ and ϵ, and it is described by

$$\{\Lambda, \Lambda^*\} \sim \mathrm{Pe}^{-\alpha} \tag{19}$$

for over six orders of magnitude in Pe. Furthermore, $\alpha \approx 0.75$ for Λ at higher fill fractions, while $\alpha \approx 0.5$ for Λ^*. This is similar to the separation of scalings observed for the branches of real and complex eigenvalues of the Floquet operator corresponding to the idealized time-periodic sine flow.[67]

Note that we have excluded the case of $\epsilon = 0$ in middle panel of Fig. 14(b) because there are no complex eigenvalues for this choice of (ϕ, ϵ). The modified mapping matrix $\widetilde{\boldsymbol{\Phi}}$ only has two distinct eigenvalues: 1 and -1. Therefore, Λ^* does not exist for this choice of ϕ and ϵ. Furthermore, the advection part of this advection-diffusion process is trivial as

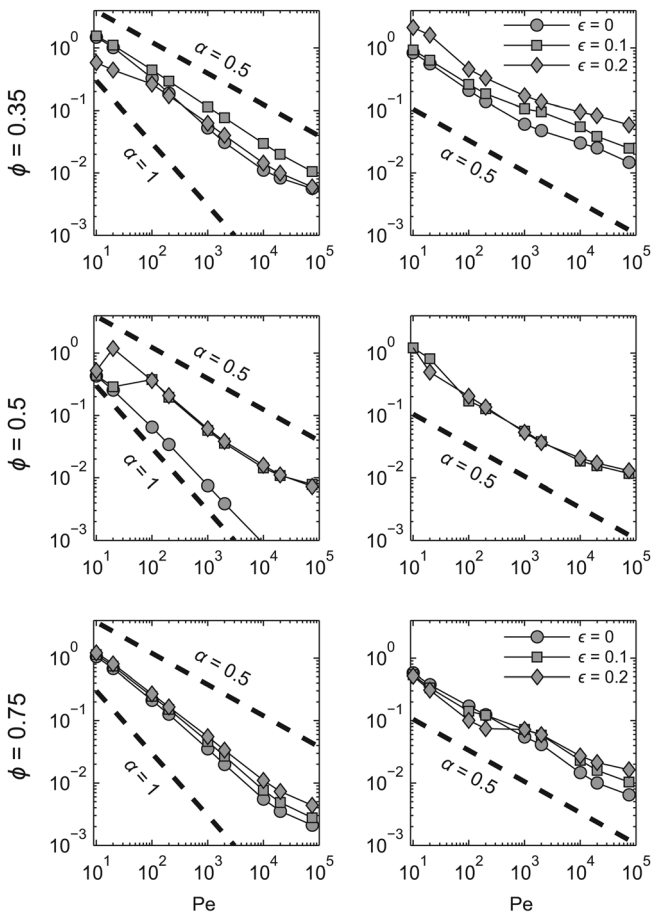

FIG. 14. Scaling of the dominant exponents of $\widetilde{\mathbf{\Phi}}$ with the Péclet number for $\phi = 0.35$ (top), $\phi = 0.5$ (middle), and $\phi = 0.75$ (bottom).

shown by the rightmost column of Fig. 4. For these same reasons, whenever the mapping matrix is modified due to diffusion, we then observe "perfect" Pe^{-1} scaling for this (ϕ, ϵ) pair in middle panel of Fig. 14(a), unlike what is seen for other values of ϵ and $\phi = 0.5$.

Another way to frame the results in Fig. 14 is that advection, which is always at least partially chaotic for the parameters considered here, generates strange eigenmodes (specifically, ones with complex eigenvalues), and the resulting complicated spatial structure allows diffusion to "work faster" leading to *convection-enhanced diffusion*[68] and the $\mathrm{Pe}^{-1/2}$ scaling for Λ^* in a granular flow. To make this clear, note that if $\{\Lambda,\Lambda^*\}\sim\mathrm{Pe}^{-\alpha}$, then their respective $\{\tau_k,\tau_k^*\} \sim \mathrm{Pe}^{\alpha}$. Therefore, $\tau_k^* \sim \sqrt{\mathrm{Pe}} < \mathrm{Pe} \sim \tau_k$ (when $\mathrm{Pe} > 1$), meaning the lifespan of the strange/oscillatory eigenmodes generated by advection is shorter than any purely diffusive ones. Furthermore, for the real branch of eigenvalues, the dominant exponent Λ scales closer to $\mathrm{Pe}^{-1/2}$ at the lower fill fraction (35%) than at the higher fill fractions (50%, 75%). This can be explained by noting that for $\phi < 0.5$, all material in the container goes through the flowing layer (where stretching occurs), and particles make a complete circuit through the filled portion more times per period than at higher fill fractions. In turn, this can lead to more filamentary structures and intermaterial interfaces and, hence, the enhancement in the scaling observed.

D. Lifespan of a granular strange eigenmode

In this section, we present an exploratory analysis on the connection between eigenmodes of the Floquet advection-diffusion operator stemming from Eq. (4), with the velocity field given by Eq. (1), and granular mixing and segregation patterns in a rotating tumbler. Figure 15 shows a comparison between the evolution of a bidisperse mixing experiment (left column, see Appendix A), a monodisperse mixing experiment (second column, in fact, the one from Fig. 6 for larger n) and direct sums of two dominant eigenmodes from Fig. 13 (third and fourth columns). First, we note that no attempt is made to combine the eigenmodes so as to reproduce a specific pattern or initial condition. Rather, we have chosen ones that are excited in the experiments and are

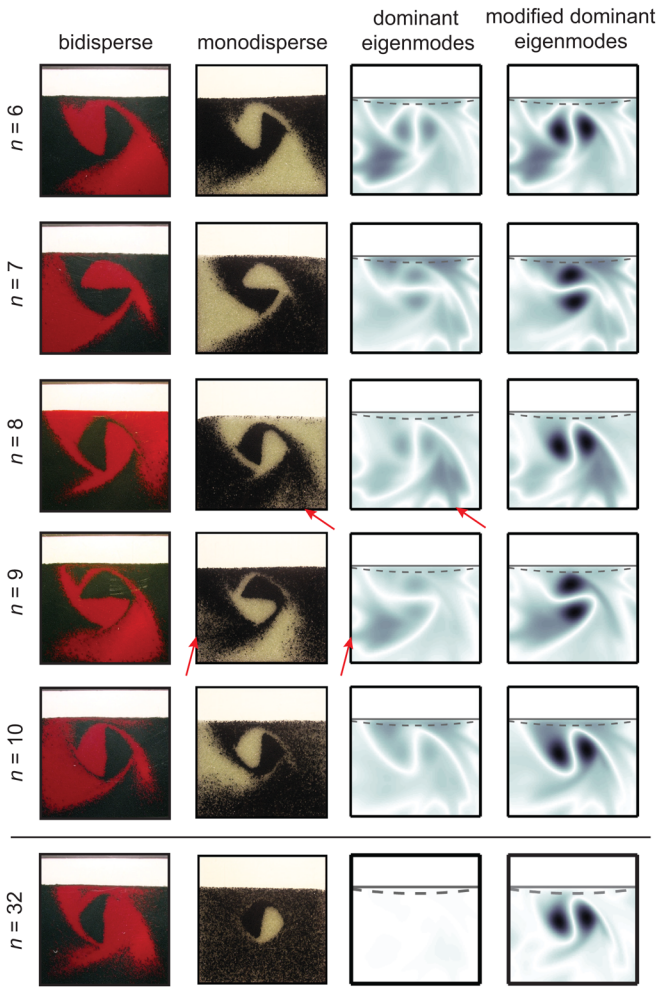

FIG. 15. (Color online) At moderate numbers of revolutions, beyond those considered in Fig. 6, the excited most dominant period-3 and period-4 eigenmodes can be observed in both bidisperse (first column) and monodisperse (second column) granular mixing experiments. To illustrate their periodicities and decay, the third column is a direct superposition of two dominant eigenmodes from Fig. 13 ($\phi = 0.75$, $\epsilon = 0.1$, and $\mathrm{Pe} = 10{,}000$), specifically $|\hat{\psi}_4(\boldsymbol{x};n) + \hat{\psi}_{10}(\boldsymbol{x};n)|$. Meanwhile, the fourth column is an *ad-hoc* modification, i.e., $|\hat{\psi}_4(\boldsymbol{x};n) + \mathrm{i}^n\hat{\psi}_{10}(\boldsymbol{x};0)|$, to account for the persistent unmixed core in the experiments. Color scale for the eigenmodes is normalized with respect to their magnitude at $n = 0$. At $n = 32$, the magnitude of the eigenmodes in the third column has decayed to 5% of the initial one, so the pattern is barely visible. Meanwhile, because we modified the eigenvalue μ_{10} in the fourth column, the magnitude of the eigenmode related to the unmixed core does not decay.

immediately identifiable visually. Specifically, a period-4 eigenmode in the solid core and a period-3 eigenmode related to the KAM islands (located on the main diagonals of the tumbler at this fill fraction) are superimposed. The latter is particularly easy to observe at $n=8$ and 9 because its active region has a protrusion reaching out towards the tumbler wall, as noted by the arrows in Fig. 15. This is also where particles in the experiment migrate.

In Sec. V C, we argued that diffusion makes the lifespan of even the most dominant (inhomogeneous) strange eigenmodes finite. Indeed, Fig. 15 shows that by $n=32$, the intensity of the combination of the eigenmodes shown in the third column has decayed to the point of being indistinguishable. Similarly, in the monodisperse experiment, the granular material appears well-mixed, aside from the solid core. Note that the core never goes through the flowing layer and thus does not experience the same kind of granular diffusion as the rest of the material. Although it is slowly eroded at higher numbers of periods,[69] one way to properly account (through Eq. (4a)) for its "different" diffusion characteristics might be to introduce an inhomogeneous diffusion coefficient $D=D(\boldsymbol{x})$, whose construction would require further modeling assumptions. Alternatively, for illustration purposes, we can modify the eigenvalue of the eigenmode corresponding to the period rotation of the core from $\mu_{10}=-0.0184+0.888\mathrm{i}$ to $\mu_{10}=\mathrm{i}$. This *ad-hoc* modification makes the eigenmode corresponding to the persistent unmixed core non-decaying, as illustrated in the fourth column of Fig. 15.

Unlike fluid-fluid mixing experiments, granular mixing presents the possibility of *segregation* in a bidisperse mixture.[1,2,24–27] As the first column of Fig. 15 shows, it is possible to use segregation to force a few dominant eigenmodes indefinitely, in a sense approximately "canceling out" the effect of diffusion on their lifespan.

Such a connection between the kinematic scalar transport description, which requires only the specification of the velocity field in the tumbler, can predict *a priori* the types of segregation patterns one can expect. The connection becomes clearer when one recalls the observation of Voth *et al.*[15,16] (and a similar one for turbulent velocity fields[70,71]) that the spatial gradient of a strange eigenmode tends to align with the ridges of the stretching (FTLE) field, which the discussion in Sec. V A corroborates. The curves of largest local stretching, in turn, can be shown to be parts of the unstable manifold(s) of hyperbolic periodic point(s) of the dynamical system generated by the velocity field (Eq. (1)) of the flow under consideration. Finally, finite-length traces of unstable manifolds of hyperbolic periodic points have been shown to outline the segregation pattern because they are barriers to transport once segregation has taken place.[25]

Here, the eigenmode picture of segregation has an advantage: it can describe the internal structure of the pattern not just its outer boundary. Unlike experiments on strange eigenmodes in fluids,[14,17] due to the prominent effect of granular diffusion, we cannot observe the concentration profile saturating to a long-lived combination of eigenmodes in a monodisperse experiment. However, as a comparison of the segregation pattern in the bidisperse experiment at $n=32$ in the left column of Fig. 15 and the combination of eigenmodes in the third and fourth columns at $n=8$ (to account for periodicities) makes clear, eigenmodes can be permanently excited using a bidisperse mixture that is capable of segregating.

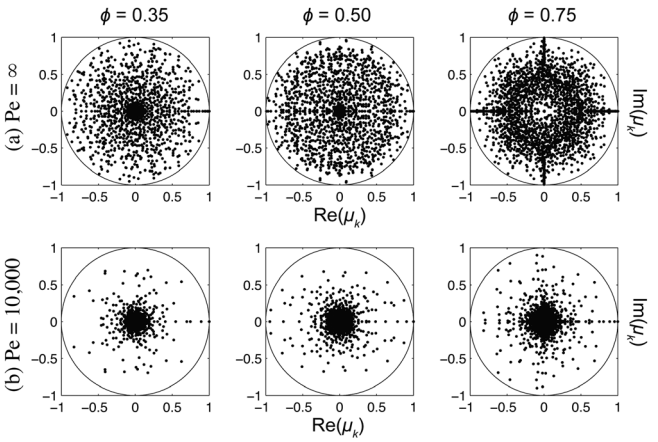

FIG. 16. Spectra of $\widetilde{\boldsymbol{\Phi}}$, the mapping method approximation to the Floquet operator $\mathcal{F}$, in the complex plane for (a) $\mathrm{Pe}=\infty$ and (b) $\mathrm{Pe}=10{,}000$ and three different fill fractions: $\phi=0.35$ (left), $\phi=0.5$ (center), and $\phi=0.75$ (right). Diffusion shrinks the spectrum significantly leaving only a small number of dominant strange eigenmodes. The flowing layer aspect ratio is $\epsilon=0.1$ for all cases.

To give further insight into the lifespan of eigenmodes, we present in Fig. 16 plots of the eigenvalues of the modified mapping matrix $\widetilde{\boldsymbol{\Phi}}$ in the complex plane, for (a) purely advective and (b) advective-diffusive transport. In the case of pure advection, the spectrum fills most of the unit disk (to which all eigenvalues are restricted). This implies the existence of a large number of strange eigenmodes, i.e., ones with complex μ_k of large magnitude. These will persist for long times, impeding complete homogenization of the material. However, when diffusive effects (finite Pe) are considered, the spectrum shrinks significantly in Fig. 16(b) becoming "squished" into an elliptical shape (prominently seen for $\phi=0.35$ and $\phi=0.5$ in Fig. 16(b)), which is quite similar to Fig. 3 of Cerbelli *et al.*[40] for the case of the idealized time-periodic sine flow. Thus, the majority of eigenvalues are now within the disk $|\mu_k|\lesssim 0.5$. The corresponding eigenmodes will decay rapidly in time without affecting mixing significantly. Specifically, the number of periods required for an eigenmode to lose half its initial magnitude is n such that $|\mu_k|^n=0.5|\mu_k|^0=0.5$, or $n=\ln(0.5)/\ln|\mu_k|$, which gives $n\approx 1$ for $|\mu_k|\approx 0.5$.

Nevertheless, from the spectrum plot, a few strange eigenmodes are still expected. For example, most of the eigenvalues for $\mathrm{Pe}=10{,}000$ and $\phi=0.75$ are distributed along the real and imaginary axis, which would corresponding to period-4 structures (the fourth roots of unity being $\{1,\mathrm{i},-1,-\mathrm{i}\}$). In Sec. V B and Fig. 13, we observed that the period-4 eigenmodes that correspond to the unmixed core present in the tumbler at this fill fraction remain dominant in the presence of diffusion. Similarly, for the case of pure advection in Fig. 16(a), the clustering of eigenvalues along the real and imaginary axes correlates with the noticeable number of period-4 orbits in the corresponding Poincaré section in Fig. 8(b).

Finally, we have been unable to find parameters (i.e., a fill fraction ϕ for a given ϵ) for our granular flow that significantly shrink the spectrum of the pure-advection mapping matrix as was done by Singh *et al.*[19] for the idealized time-periodic sine flow (see, e.g., Fig. 4 therein). This highlights the importance of diffusion in granular mixing. The stirring induced by tumbling is itself insufficient to lead to thorough mixing because KAM islands are generic in this granular flow.

VI. CONCLUSIONS AND OUTLOOK

The present work has focused on three aspects of granular flow in slowly rotating tumbling mixers: the short-time vanishing-flowing-layer kinematics, the presence of strange eigenmodes generated by the underlying velocity field in the tumbler, and the effects on the latter due to diffusion from inter-particle collision in the flowing layer. Our analysis also emphasized the unity between the Lagrangian and Eulerian descriptions of granular mixing by relating the features of Lagrangian flow structures to those of Eulerian eigenmodes, strengthening previous results on this connection for two-dimensional fluid mixing experiments.[15,16]

Specifically, we have provided experimental evidence that streamline jumping, that is the mechanism of mixing in the absence of stretching and folding or diffusion in the flowing layer, can be readily observed as the skeleton of the mixing pattern in experiments for low numbers of revolutions. We have shown that strange eigenmodes are excited in granular mixing experiments, though diffusion leads to a much faster decay of their amplitudes than in fluid mixing experiments, leading to quick homogenization (outside of the unmixed core present at fill levels $\gtrsim 50\%$) of the material. The latter is done through a simple modification of the mapping method for scalar transport that makes it possible to study, computationally, the change in structure and lifetime of granular strange eigenmodes. Finally, we have established that segregation can lead to permanent excitation of dominant eigenmodes. Thus, it appears that the "internal" Eulerian structure of segregation patterns can be understood through eigenmode analysis, much like their shape (outline) can be understood from manifold analysis.

Much remains to be done, however. In the future, it would be useful to develop further the numerical approximation properties of our modification of the simplified mapping method, and of the simplified mapping method itself. Specifically, comparing such particle-based methods to those[72] that directly approximate the partial differential equation (4a). In addition, it would be useful to establish to what extent the modified mapping matrix $\widetilde{\mathbf{\Phi}}$ constitutes a discrete approximation of some abstract operators from dynamical systems theory, e.g., the Ulam transfer operator,[73–75] the Perron–Frobenius operator[64,74–76] or the Koopman operator.[77,78] In fact, while our discussion is grounded in the language of continuum mechanics, others have recently presented mathematical studies of idealized flows in which eigenmodes are referred to as "almost-invariant"[73,74] or "almost-cyclic"[75] sets, with the Lagrangian and Eulerian descriptions being termed the "geometric" and "probabilistic" ones, respectively.[74]

Another important question to be addressed is whether one should consider the *pseudospectra*[79] of the advection-diffusion Floquet operator $\mathcal{F}$ rather than its proper spectrum. The operator $\mathcal{F}$ is not self-adjoint, and its numerical analogue $\widetilde{\mathbf{\Phi}}$ studied here is not even a normal matrix. Although we have obtained good results that match the experimental data, depending on how "far from normal" $\widetilde{\mathbf{\Phi}}$ is, its eigenvalues and eigenvectors may or may not be a good representation of the behavior of $\widetilde{\mathbf{\Phi}}^n$, which (as we have argued) is an approximation to n periods of the time-periodic advection-diffusion granular mixing process.

ACKNOWLEDGMENTS

We would like to thank Gabriel Juarez for helpful discussions on the material in Section III. The images of the monodisperse and bidisperse experiments were kindly provided by Emre Yildiz and Florent Pignatel, respectively. The careful reading and insightful comments by the referees are much appreciated. This work was supported, in part, by NSF Grant CMMI-1000469. ICC was also supported, in part, by a Walter P. Murphy Fellowship from the Robert R. McCormick School of Engineering and Applied Science at Northwestern University.

APPENDIX A: EXPERIMENTAL METHODS

We used the same apparatus as in Refs. 24 and 25 with a tumbler of side length $S = 25$ cm and thickness in the axial direction $W = 12$ mm. The tumbler was attached to a computer-controlled stepper motor and was rotated clockwise about the geometric centroid of its face at 1 revolution per minute (RPM), nearly the slowest possible rotation rate (of this apparatus) before switching from continuous flow to avalanching. Images of the tumbler were taken with a digital camera. For the monodisperse experiments, 2 mm (2.02 ± 0.05 mm) black and 2 mm (2.03 ± 0.05 mm) clear glass beads with equal densities were used. Meanwhile, for the bidisperse experiments, 2 mm (2.03 ± 0.05 mm) black and 1 mm (1.06 ± 0.08 mm) clear glass beads dyed red with equal densities were used. To produce a half-and-half initial condition, a divider was placed down the centerline of the tumbler and equal volumes ($= 0.5\phi D^2$, where ϕ is the fill fraction) of particles poured on each side. The divider was carefully removed so that particles underwent minimal rearrangement.

APPENDIX B: COMPUTATIONAL METHODS

The numerical simulations presented in Sec. III were performed as follows. We simulated granular flow in a convex tumbling container by advecting a fine uniform grid of tracer particles (material points of the continuum) backwards in time by a given number of flow periods, then we colored the initial uniform grid based on whether the x-coordinate of the point after the backward iteration was positive or negative. This is because we chose the initial condition in all simulations and experiments to be such that $x < 0$ corresponds to light gray/clear material, while $x \geq 0$ corresponds to black material. In this manner, the spacing between particles in the final plot is uniform, which would not be the case if we first

assigned a color to them and advected them forward in time for the given number of flow periods. A total of 44,100 (210×210, uniformly distributed in the x- and y-directions within the filled area of the tumbler) passive tracers (half gray, half black) were advected (see Refs. 6 and 24 for details of the numerical procedure) over 10 flow periods.

For the eigenmode analysis of the advection-diffusion problem in Secs. V A and V B, we used a grid with $N_x = N_y = 100$ cells (except for generating Fig. 16, where $N_x = N_y = 50$ was used). In each cell, 10^2 particles were seeded and tracked in order to build the mapping matrix. Eigenvalues/vectors of the modified mapping matrix $\widetilde{\mathbf{\Phi}}$ were computed with MATLAB's eigs function, which uses ARPACK's Arnoldi-based iterative solvers, to solve the generalized eigenvalue problem $\mathbf{\Phi}\psi_k = \mu_k(\mathbf{I} - T\mathrm{Pe}^{-1}\Delta^h)\psi_k$. By doing so, we avoided having to perform the possibly computationally intensive matrix inversion in Eq. (15), which could have led to a worse-conditioned, though normal, eigenvalue problem.

[1] K. M. Hill, D. V. Khakhar, J. F. Gilchrist, J. J. McCarthy, and J. M. Ottino, "Segregation-driven organization in chaotic granular flows," Proc. Natl Acad. Sci. USA **96**, 11701 (1999).
[2] I. S. Aranson and L. S. Tsimring, *Granular Patterns* (Oxford University Press, New York, 2009).
[3] G. Juarez, R. M. Lueptow, J. M. Ottino, R. Sturman, and S. Wiggins, "Mixing by cutting and shuffling," Europhys. Lett. **91**, 20003 (2010).
[4] T. Elperin and A. Vikhansky, "Chaotic mixing of granular material in slowly rotating containers as a discrete mapping," Chaos **9**, 910 (1999).
[5] I. C. Christov, J. M. Ottino, and R. M. Lueptow, "Streamline jumping: A mixing mechanism," Phys. Rev. E **81**, 046307 (2010).
[6] I. C. Christov, J. M. Ottino, and R. M. Lueptow, "Chaotic mixing via streamline jumping in quasi-two-dimensional tumbled granular flows," Chaos **20**, 023102 (2010).
[7] A. Goetz, "Dynamics of a piecewise rotation," Discr. Cont.. Dyn. Syst. A **4**, 593 (1998).
[8] A. Goetz, "Piecewise isometries—an emerging area of dynamical systems," in *Fractals in Graz 2001*, edited by P. Grabner and W. Woess (Birkhäuser, Basel, 2002), pp. 135–144.
[9] J. H. B. Deane, "Piecewise isometries: Applications in engineering," Meccanica **41**, 241 (2006).
[10] B. Kahng, "Singularities of two-dimensional invertible piecewise isometric dynamics," Chaos **19**, 023115 (2009).
[11] I. C. Christov, R. M. Lueptow, and J. M. Ottino, "Stretching and folding versus cutting and shuffling: An illustrated perspective on mixing and deformations of continua," Am. J. Phys. **74**, 359 (2011).
[12] J. M. Ottino, C. W. Leong, H. Rising, and P. D. Swanson, "Morphological structures produced by mixing in chaotic flows," Nature **333**, 419 (1988).
[13] R. T. Pierrehumbert, "Tracer microstructure in the large-eddy dominated regime," Chaos Solitons Fractals **4**, 1091 (1994).
[14] D. Rothstein, E. Henry, and J. P. Gollub, "Persistent patterns in transient chaotic fluid mixing," Nature **401**, 770 (1999).
[15] G. A. Voth, G. Haller, and J. P. Gollub, "Experimental measurements of stretching fields in fluid mixing," Phys. Rev. Lett. **88**, 254501 (2002).
[16] G. A. Voth, T. C. Saint, G. Dobler, and J. P. Gollub, "Mixing rates and symmetry breaking in two-dimensional chaotic flow," Phys. Fluids **15**, 2560 (2003).
[17] E. Gouillart, O. Dauchot, J.-L. Thiffeault, and S. Roux, "Open-flow mixing: Experimental evidence for strange eigenmodes," Phys. Fluids **21**, 023603 (2009).
[18] W. Liu and G. Haller, "Strange eigenmodes and decay of variance in the mixing of diffusive tracers," Physica D **188**, 1 (2004).
[19] M. K. Singh, M. F. M. Speetjens, and P. D. Anderson, "Eigenmode analysis of scalar transport in distributive mixing," Phys. Fluids **21**, 093601 (2009).
[20] R. S. Spencer and R. M. Wiley, "The mixing of very viscous liquids," J. Colloid Sci. **6**, 133 (1951).
[21] M. K. Singh, O. S. Galaktionov, H. E. H. Meijer, and P. D. Anderson, "A simplified approach to compute distribution matrices for the mapping method," Comput. Chem. Eng. **33**, 1354 (2009).
[22] D. V. Khakhar, J. J. McCarthy, J. F. Gilchrist, and J. M. Ottino, "Chaotic mixing of granular materials in two-dimensional tumbling mixers," Chaos **9**, 195 (1999).
[23] R. Hogg and D. Fuerstenau, "Transverse mixing in rotating cylinders," Powder Technol. **6**, 139 (1972).
[24] S. E. Cisar, P. B. Umbanhowar, and J. M. Ottino, "Radial granular segregation under chaotic flow in two-dimensional tumblers," Phys. Rev. E **74**, 051305 (2006).
[25] S. W. Meier, S. E. Cisar, R. M. Lueptow, and J. M. Ottino, "Capturing patterns and symmetries in chaotic granular flow," Phys. Rev. E **74**, 031310 (2006).
[26] G. H. Ristow, *Pattern Formation in Granular Materials* (Springer-Verlag, Berlin, 2000).
[27] S. W. Meier, R. M. Lueptow, and J. M. Ottino, "A dynamical systems approach to mixing and segregation of granular materials in tumblers," Adv. Phys. **56**, 757 (2007).
[28] G. Metcalfe, T. Shinbrot, J. J. McCarthy, and J. M. Ottino, "Avalanche mixing of granular solids," Nature **374**, 39 (1995).
[29] J. J. McCarthy, T. Shinbrot, G. Metcalfe, J. E. Wolf, and J. M. Ottino, "Mixing of granular materials in slowly rotated containers," AIChE J. **42**, 3351 (1996).
[30] D. V. Khakhar, J. J. McCarthy, T. Shinbrot, and J. M. Ottino, "Transverse flow and mixing of granular materials in a rotating cylinder," Phys. Fluids **9**, 31 (1997).
[31] J. Rajchenbach, "Flow in powders: From discrete avalanches to continuous regime," Phys. Rev. Lett. **65**, 2221 (1990).
[32] R. Fischer, P. Gondret, and M. Rabaud, "Transition by intermittency in granular matter: From discontinuous avalanches to continuous flow," Phys. Rev. Lett. **103**, 128002 (2009).
[33] B. A. Peratt and J. A. Yorke, "Continuous avalanche mixing of granular solids in a rotating drum," Europhys. Lett. **35**, 31 (1996).
[34] T. Elperin and A. Vikhansky, "Kinematics of the mixing of granular material in slowly rotating containers," Europhys. Lett. **43**, 17 (1998).
[35] N. Jain, J. M. Ottino, and R. M. Lueptow, "Effect of interstitial fluid on a granular flowing layer," J. Fluid Mech. **508**, 23 (2004).
[36] P. M. C. Lacey, "Developments in the theory of particle mixing," J. Appl. Chem. **4**, 257 (1954).
[37] To see why it could be either, let $c = c_b$ (i.e., c is the concentration of black particles), then by conservation of mass $c_b + c_w = 1$, where c_w is the concentration of clear particles. Hence, $c_w = 1 - c_b$, and it is evident that c_w thus satisfies the boundary value problem in Eq. (4) as well.
[38] J.-L. Thiffeault, "Scalar decay in chaotic mixing," Lect. Notes Phys. **744**, 3 (2008).
[39] D. R. Lester, M. Rudman, G. Metcalfe, and H. M. Blackburn, "Global parametric solutions of scalar transport," J. Comput. Phys. **227**, 3032 (2008).
[40] S. Cerbelli, V. Vitacolonna, A. Adrover, and M. Giona, "Eigenvalue–eigenfunction analysis of infinitely fast reactions and micromixing regimes in regular and chaotic bounded flows," Chem. Eng. Sci. **59**, 2125 (2004).
[41] S. Cerbelli, A. Adrover, F. Creta, and M. Giona, "Foundations of laminar chaotic mixing and spectral theory of linear operators," Chem. Eng. Sci. **61**, 2754 (2006).
[42] C. I. Christov and G. M. Homsy, "Enhancement of transport from drops by steady and modulated electric fields," Phys. Fluids **21**, 083102 (2009).
[43] D. R. Lester, M. Rudman, and G. Metcalfe, "Low Reynolds number scalar transport enhancement in viscous and non-Newtonian fluids," Int. J. Heat Mass Transfer **52**, 655 (2009).
[44] D. R. Lester, M. Rudman, G. Metcalfe, M. G. Trefry, A. Ord, and B. Hobbs, "Scalar dispersion in a periodically reoriented potential flow: Acceleration via lagrangian chaos," Phys. Rev. E **81**, 046319 (2010).
[45] K. El Omari and Y. Le Guer, "Alternate rotating walls for thermal chaotic mixing," Int. J. Heat Mass Transfer **53**, 123 (2010).
[46] In general (i.e., off the inertial manifold), this equality is always only approximate because, in the non-autonomous case, the eigenfunctions of $\mathcal{L}$ are not complete except for the limiting case of $\mathrm{Pe} = 0$ when the operator is self-adjoint. It can be shown, however, that for a time-periodic velocity field, as in the present work, the neglected terms are *exponentially small* (Theorem 4 of Liu and Haller[18]).
[47] J. G. Franjione and J. M. Ottino, "Feasibility of numerical tracking of material lines and surfaces in chaotic flows," Phys. Fluids **30**, 3641 (1987).
[48] P. D. Anderson and H. E. H. Meijer, "Chaotic mixing analyses by distribution matrices," Appl. Rheol. **10**, 119 (2000).
[49] P. G. M. Kruijt, O. S. Galaktionov, P. D. Anderson, G. W. M. Peters, and H. E. H. Meijer, "Analyzing mixing in periodic flows by distribution matrices: Mapping method," AIChE J. **47**, 1005 (2001).

[50]O. S. Galaktionov, P. D. Anderson, G. W. M. Peters, and C. L. Tucker III, "A global, multi-scale simulation of laminar fluid mixing: the extended mapping method," Int. J. Multiphase Flow **28**, 497 (2002).
[51]M. K. Singh, T. G. Kang, H. E. H. Meijer, and P. D. Anderson, "The mapping method as a toolbox to analyze, design, and optimize micromixers," Microfluid. Nanofluid. **5**, 313 (2008).
[52]R. Glowinski, "Finite element methods for incompressible viscous flow," in *Numerical Methods for Fluids (Part 3)*, Handbook of Numerical Analysis Vol. 9, edited by P. G. Ciarlet and J. L. Lions (Elsevier, Amsterdam, 2003).
[53]P. Knabner and L. Angermann, *Numerical Methods for Elliptic and Parabolic Partial Differential Equations*, Texts in Applied Mathematics, Vol. 44 (Springer, Berlin, 2003).
[54]The matrix $\mathbf{\Phi}$ represents an unconditionally stable approximation to the operator $(\boldsymbol{I} - T\mathcal{L}_1^h)^{-1}$ from the advection step because $\| \mathbf{\Phi} \|_2 = 1$, where $\| \cdot \|_2$ is the spectral norm.
[55]Y. Du and E. Ott, "Fractal dimensions of fast dynamo magnetic fields," Physica D **67**, 387–417 (1993).
[56]H. Aref, "Stirring by chaotic advection," J. Fluid Mech. **143**, 1 (1984).
[57]J. M. Ottino, *The Kinematics of Mixing: Stretching, Chaos, and Transport* (Cambridge University Press, Cambridge, 1989).
[58]G. Haller, "Distinguished material surfaces and coherent structures in three-dimensional fluid flows," Physica D **149**, 238 (2001).
[59]S. C. Shadden, F. Lekien, and J. E. Marsden, "Definition and properties of Lagrangian coherent structures from finite-time Lyapunov exponents in two-dimensional aperiodic flows," Physica D **212**, 271 (2005).
[60]G. Haller and G. Yuan, "Lagrangian coherent structures and mixing in two-dimensional turbulence," Physica D **147**, 352 (2000).
[61]G. Haller, "A variational theory of hyperbolic Lagrangian coherent structures," Physica D **240**, 574 (2011).
[62]G. Haller, "Lagrangian coherent structures from approximate velocity data," Phys. Fluids **14**, 1851 (2002).
[63]Interpreting the mapping method as a numerical method for solving an advection equation, it is clear that it must introduce some "numerical diffusion" into the solution. In other words, since only a finite number of cells are used, the fine-scale features that (chaotic) advection can generate cannot be resolved, that is they become "diffused." Singh *et al.*[19] discuss some of the consequences of numerical diffusion on the eigenmode analysis of scalar transport. Here, it suffices to note that doubling the resolution of the grid from $N_x = N_y = 50$ to $N_x = N_y = 100$ changes the magnitude of, e.g., $\mu_{4,5}$ from ≈ 0.980823 to ≈ 0.994591, an almost four-fold decrease in the "error" (i.e., difference from 1) suggesting better than first-order convergence toward the true value.
[64]O. V. Popovych, A. Pikovsky, and B. Eckhardt, "Abnormal mixing of passive scalars in chaotic flows," Phys. Rev. E **75**, 036308 (2007).
[65]S. B. Savage, "Disorder, diffusion, and structure formation in granular flow," in *Disorder and Granular Media*, edited by A. Hansen and D. Bideau (Elsevier, Amsterdam, 1993), pp. 255–285.
[66]S. W. Jones, "The enhancement of mixing by chaotic advection," Phys. Fluids A **3**, 1081 (1991).
[67]M. Giona, A. Adrover, S. Cerbelli, and V. Vitacolonna, "Spectral properties and transport mechanisms of partially chaotic bounded flows in the presence of diffusion," Phys. Rev. Lett. **92**, 114101 (2004).
[68]A. Fannjiang and G. Papanicolaou, "Convection enhanced diffusion for periodic flows," SIAM J. Appl. Math **54**, 333 (1994).
[69]B. A. Socie, P. B. Umbanhowar, R. M. Lueptow, N. Jain, and J. M. Ottino, "Creeping motion in granular flow," Phys. Rev. E **71**, 031304 (2005).
[70]G. Lapeyre, P. Klein, and B. L. Hua, "Does the tracer gradient vector align with the strain eigenvectors in 2D turbulence?" Phys. Fluids **11**, 3729 (1999).
[71]P. Klein, B. L. Hua, and G. Lapeyre, "Alignment of tracer gradient vectors in 2D turbulence," Physica D **146**, 246 (2000).
[72]A. Chertock, C. R. Doering, E. Kashdan, and A. Kurganov, "A fast explicit operator splitting method for passive scalar advection," J. Sci. Comput. **45**, 200 (2010).
[73]G. Froyland, K. Padberg, M. H. England, and A. M. Treguier, "Detection of coherent oceanic structures via transfer operators," Phys. Rev. Lett. **98**, 224503 (2007).
[74]G. Froyland and K. Padberg, "Almost-invariant sets and invariant manifolds – Connecting probabilistic and geometric descriptions of coherent structures in flows," Physica D **238**, 1507 (2009).
[75]M. A. Stremler, S. D. Ross, P. Grover, and P. Kumar, "Topological chaos and periodic braiding of almost-cyclic sets," Phys. Rev. Lett. **106**, 114101 (2011).
[76]A. Pikovsky and O. Popovych, "Persistent patterns in deterministic mixing flows," Europhys. Lett. **61**, 625 (2003).
[77]I. Mezić, "Spectral properties of dynamical systems, model reduction and decompositions," Nonlinear Dyn. **41**, 309 (2005).
[78]C. W. Rowley, I. Mezić, S. Bagheri, P. Schlatter, and D. S. Henningson, "Spectral analysis of nonlinear flows," J. Fluid Mech. **641**, 115 (2009).
[79]L. N. Trefethen and M. Embree, *Spectra and Pseudospectra* (Princeton University Press, Princeton, NJ, 2005).